This is a post-peer-review, pre-copyedit version of an article published in Construction and Building Materials. The final authenticated version is available online at: https://doi.org/10.1016/j.conbuildmat.2021.124962

Low-impact techniques for seismic strengthening fair faced masonry walls

Stefano De Santis[1a], Omar AlShawa[2b], Gianmarco de Felice[1c], Francesca Gobbin[1d], Ivan Roselli[3e], Marialuigia Sangirardi[1f], Luigi Sorrentino[2g*], Domenico Liberatore[2h]

[1] Roma Tre University, Department of Engineering, *Via Vito Volterra 62, 00146 Rome, Italy*.
[2] Sapienza University of Rome, Department of Structural and Geotechnical Engineering, *Via Antonio Gramsci 53, 00197 Rome, Italy*.
[3] ENEA Centro Ricerche Casaccia, Laboratorio Tecnologie per la Dinamica delle Strutture e la Prevenzione del rischio sismico e idrogeologico, *Via Anguillarese 301, 00123 Santa Maria di Galeria, Rome, Italy*.

[a] E: stefano.desantis@uniroma3.it. ORCID: 0000-0002-0816-4865.
[b] E: omar.alshawa@uniroma1.it. ORCID: 0000-0001-7905-5482.
[c] E: gianmarco.defelice@uniroma3.it. ORCID: 0000-0002-0917-0220.
[d] E: francesca.gobbin@uniroma3.it. ORCID: 0000-0002-2596-8355.
[e] E: ivan.roselli@enea.it. ORCID: 0000-0003-4984-2156.
[f] E: marialuigia.sangirardi@uniroma3.it. ORCID: 0000-0002-9920-7380.
[g] E: luigi.sorrentino@uniroma1.it. ORCID: 0000-0003-1652-942X.
[h] E: domenico.liberatore@uniroma1.it. ORCID: 0000-0003-3184-8189.

* Corresponding Author. T: +39 06 49919186, F: +39 06 49919183.

HIGHLIGHTS

- Two strengthening techniques for masonry walls were tested on a shake table.
- CFRP connectors are installed from the outside leaving the internal face undisturbed.
- Joint repointing with stainless steel cords and thermo-insulating CRM were coupled.
- Seismic capacity of walls was enhanced avoiding leaf separation and disintegration.
- Both techniques have low impact and preserve the fair face of stone masonry façades.

ABSTRACT

Two techniques for the seismic strengthening of fair faced rubble masonry walls are proposed and tested on a shake table. The first solution entails the use of carbon fibre reinforced polymer connectors installed from outside through the natural stone units, without perforating the entire wall thickness, thus leaving the internal wall surface undisturbed. In the second solution, stainless-steel cords are embedded in repointed mortar joints of the fair face and connected, by means of stainless-steel bars, to a thermo-insulating composite reinforced mortar applied to the internal side. Shake table tests were performed under natural accelerograms on real scale multi-leaf rubble masonry walls, built with the stone units retrieved from the debris of a hamlet heavily damaged in the 2016 Central Italy earthquakes. Both strengthening solutions proved effective in enhancing the seismic capacity by preventing leaf separation and masonry disintegration, and in limiting damage development under earthquake excitation. Thanks to the compatibility with original materials and the preservation of the fair face, they are suitable for mitigating the seismic vulnerability of architectural heritage.

Keywords

2016-2017 Central Italy earthquakes; 3DVision; Carbon fibre reinforced polymer (CFRP); Composite connectors; Composite reinforced mortar (CRM); Mortar-based composites; Mortar joint repointing; Stainless-steel; Natural accelerogram; Shake table tests.

1. INTRODUCTION

In many countries a significant proportion of the historical centres is built with rubble stone masonry. In case of an earthquake, the irregular arrangement of the bond pattern, the poor quality of the mortar, and the weak connection with orthogonal walls and horizontal structures (floor, roof) are responsible of ruinous collapses by leaf separation and disintegration, especially under out of plane loads [1–5]. This damage pattern still represents a major challenge for both the scientific and engineering communities. On the one hand, the complex dynamic response of such types of masonry complicates the assessment of seismic capacity [6], especially with rigid-body mechanics approaches [7]. On the other hand, effective strengthening techniques are needed to protect human lives and safeguard the built heritage, while ensuring the conservation of its architectural value. Metallic ties and top ring beams, which have been extensively installed after past earthquakes, may not be sufficient by themselves to prevent masonry disintegration and leaf separation, so distributed strengthening systems are also needed [8–10]. Further challenges are posed to the development of improved strengthening solutions by the following additional requirements:

1) ensuring the compatibility with original materials;
2) preserving the fair face of the fair faced sides;
3) sparing, whenever possible, the occupants leaving the building and keeping its use running;
4) safeguarding a decorated side of the wall by implementing the intervention from the opposite one;
5) combining seismic-resistant performance and energy efficiency.

This work proposes and investigates two compatible low-impact techniques for the seismic strengthening of fair faced rubble masonry walls. One solution entails the use of carbon fibre reinforced polymer (CFRP) connectors installed from outside through the natural stone units without perforating the entire wall thickness, thus leaving the internal surface of the wall undisturbed. In the other one, the repointed mortar joints of the fair faced side are reinforced with stainless steel cords that are connected to a thermo-insulating composite reinforced mortar (CRM) applied to the internal side, by means of stainless-steel bars. Both techniques are conceived to contrast leaf separation and provide a distributed retaining effect to prevent masonry disintegration. At the same time, they are invisible from outside, so the architectural value of fair faced masonry is preserved.

The research was carried out within two research projects, named as SISMI (*Technologies for the safety improvement and the reconstruction of historical centres in seismic prone areas*) and SICURA (*Sustainable technologies for the seismic protection of the cultural heritage*), promoted after the 2016-2017 Central Italy earthquakes by Lazio regional government, to support scientific and technological innovation in seismic protection. Within this framework, shake table tests were performed on real scale multi-leaf rubble masonry wall specimens to investigate the seismic performance of the two proposed techniques. In order to replicate the materials and the arrangement surveyed in the villages of Central Italy struck by the earthquakes, the stone units were retrieved from the debris of a hamlet heavily damaged in the earthquakes, the mortar recipe was formulated based on samples collected in the area, and the walls were built according to construction practice (unit size and shape, bond pattern) typical of the region. The experimental setup was conceived to induce out of plane vertical bending under earthquake base motion, with a specific attention to the boundary conditions at the top of the wall. Three natural records of the 2016-2017 seismic sequence were applied in the horizontal and in the vertical directions.

As a whole, the research project included also a series of shake table tests on an unreinforced wall, which is described in depth in [11] and is recalled herein as reference. This paper describes the components of the two low-impact strengthening systems and their installation phases. The results of the shake table tests on the strengthened walls are presented and analysed to discuss the effectiveness of the techniques in limiting damage development under earthquake base excitation, preventing leaf separation and disintegration, and enhancing seismic capacity.

2. WALL SPECIMENS AND EXPERIMENTAL PROGRAMME

2.1. Wall specimens under investigation

The aforementioned projects SISMI and SICURA included shake table tests on three masonry walls, which were built using the compact marlstone units and lime mortar typical of the built heritage of the historical centres of Central Italy struck by the 2016-2017 earthquake. Professional bricklayers took care of their manufacturing according to construction practice (stone size and shape, bond pattern) typical of the area [12]. The accurate representation of the masonry types surveyed in the field is acknowledged as essential to investigate their behaviour, replicate their failure modes and assess the effectiveness of strengthening strategies [13]. One specimen (named as UR) was tested unstrengthened, whereas the other two specimens were strengthened. The wall strengthened with CFRP connectors is named as CC, whereas that strengthened with CRM and reinforced repointing is named as CR. As previously stated, the results of the shake table tests on UR wall are described in depth in [11] and are recalled herein as reference.

The walls (Figure 1) were about 500 mm thick, which is close to the average thickness surveyed in the historical centres of Central Italy [12] and 1630 mm wide. Since the out of plane response was under investigation, the width was not crucial and was defined to obtain a significant wall surface for the installation of the strengthening systems while limiting the forces requested upon the shake table and the construction costs. The height of the walls was 3730 mm, thus delivering a height/thickness ratio of about 7.5, which is common in the area [12]. The investigation of natural scale specimens made it possible to build the walls and apply the seismic inputs without scale effects.

In order to replicate the architectural characteristics of historical hamlets, the front side of the walls was in fair faced masonry (i.e., it was not covered with plaster) to represent the external side (the fair faced side), whereas the other side was finished with plaster and simulated the internal side of the construction. The plaster was approximately 30 mm thick and was made with a premixed natural hydraulic lime (NHL) low-strength mortar. Its mechanical properties, as well as those of all the other mortars used in this investigation, were determined on samples collected during construction and tested according to [14] within a week from the shake table tests. They are presented in Table 1.

The stone units were collected from some buildings of Collespada, a settlement of the municipality of Accumoli, which collapsed during the 2016-2017 earthquakes. Parallelepipeds with 50 mm × 50 mm × 150 mm sides were tested to determine the specific weight (w) and the flexural strength (f_f) [15], whereas cubes with 50 mm side were tested to derive compressive strength (f_m) [16]. The corresponding test results are shown in Table 1. The bedding mortar reproduced the composition detected by means of calcimetry in 20 samples collected in the area [17], and had one part, in weight, of lime and nine parts of sand, with a maximum particle size of 2 mm, resulting in particularly low flexural and compressive strengths (Table 1). Another consequence of such poor composition is the large coefficient of variation of strengths, between 19 and 56%, whereas that of specific weight is much smaller (1-3%). The bond pattern simulated a rubble stone, with two external leaves, a central nucleus with smaller elements and voids, and no bondstones (Figure 1a,b). The walls rested on a reinforced concrete (RC) foundation beam with 600 mm × 450 mm cross section, provided with three horizontal holes for moving the wall in the laboratory and fixing it to the shake table by means of steel I-girders and ∅ 20 mm threaded anchor bolts (Figure 1a).

A reinforced masonry top beam was built on top, with the same stone units of the wall, although arranged in a more regular bond pattern, and a modern NHL medium-strength premixed mortar (Table 1). One ply of a glass fibre reinforced polymer (GFRP) mesh with a 66 mm × 66 mm grid spacing was embedded in each of the three bed joints, to provide flexural strength (it is the same mesh used for the CRM overlay of CR wall). The crowing beam was 260 mm high and was connected to the underlying stonework by three ∅ 20 mm threaded galvanised steel bars, grouted for about 365 mm in the wall by means of a high-flow, non-shrink, cementitious mortar (Table 1, Figure 1c,d). On the internal side, the crowning beam was fully plastered (Figure 1e), whereas, on its external one, a narrow plaster band was laid to smooth the contact with the top restraint (Figure 1f). The construction, strengthening and testing phases of the walls are summarised in Table 2, where it is noted that the construction of UR wall was interrupted due to CoViD-19 restrictions. The smaller strengths measured for its bedding mortar are to be attributed to such interruption.

Table 1. Properties of stone units and of mortars.
Average values. Coefficient of variation and number of tested specimens in round brackets.
Cells have "–" if test results are unavailable and are left empty if the material was not used for the wall specimen.

Material	CC wall			CR wall			UR wall		
	w [kN/m^3]	f_f [MPa]	f_m [MPa]	w [kN/m^3]	f_f [MPa]	f_m [MPa]	w [kN/m^3]	f_f [MPa]	f_m [MPa]
Natural stone	–	–	–	25.9 (-; 4)	19.81 (-; 4)	91.45 (28%; 8)	–	–	–
Bedding mortar for stonework	17.3 (1%; 13)	0.56 (25%; 10)	1.34 (19%; 24)	17.0 (2%; 13)	0.41 (43%; 13)	1.04 (31%; 24)	16.9 (3%; 6)	0.36 (-; 4)	0.87 (56%; 10)
Internal side plaster				10.9 (-; 3)	2.64 (-; 3)	5.84 (13%; 6)	14.7 (-; 3)	2.79 (-; 3)	5.55 (8%; 6)
Injection grout[a]	15.8 (-; 1)	3.54 (-; 1)	9.75 (-; 1)	14.5 (-; 2)	3.10 (-; 2)	11.23 (-; 4)			
Vertical connector grout[a]	20.3 (-; 1)	9.35 (-; 1)	41.46 (-; 2)	20.4 (-; 2)	8.42 (-; 2)	41.14 (-; 3)	–	–	–
Horizontal connector grout	18.1 (8%; 6)	8.22 (28%; 6)	46.18 (18%; 11)	–	–	–			
Repointing mortar[b]				14.4 (-; 3)	2.91 (-; 3)	6.20 (8.7; 6)			

[a] Specimens, related to both strengthened walls, belonging to the same sample of three.
[b] Same mortar mix of reinforced masonry top beams of all walls.

Table 2. Initial-final day of significant construction phases, starting from day 1 of each wall.

Wall	Stonework	Vertical connectors	Top beam	Injections	Plaster	Strengthening	Test
CC	1-10	149	122	124	148	221-222, 225	253
CR	1-11	148	121	123	127-128	126-127, 144	156-157
UR	1, 87	92	93		101		123

Figure 1. Construction phases and details of the wall specimens: horizontal stonework layer (a), elevation of the fair faced side (b); top vertical connectors (c); reinforced masonry top beam (d); machine application of the plaster layer on the internal side (e), plaster band on the crowning beam (f). ***Pictures referred to CC wall.***

2.2. Shake table test setup and instrumentation

2.2.1 Experimental setup

The specimens and the experimental setup were designed to investigate the seismic behaviour of a vertical spanning wall, resting on a foundation and restrained at the top (e.g., by the connection to a floor or a roof), such that the inertial forces activated by earthquake base motion caused out-of-plane vertical bending, similarly to the investigations carried out in [13,18–22]. For this purpose, two braced steel frames were placed on the shake table on the sides of the wall (Figure 2a). Two I-girders, supported by the frames, were placed on the front and on the back side of the wall, at the height of the crowning beam. Two low-friction rubber rollers per side, fixed to the I-girders, were put in contact with the top beam. Such top restraint left vertical displacements and rotations free and prevented overturning while maintaining some flexibility in the horizontal out of plane direction. The top constraint stiffness, based on the literature values collected by [23], range from about 300 kN/m (large-size vintage floors tested in situ) to about 3400 kN/m (regular-size floors tested in the laboratory). Larger values, up to about 15 000 kN/m, were measured only for regular-size floors with plywood overlays. Accordingly, the three walls were tested under the same base excitations and using the same setup, with the only exception of a minor modification of the top restraint. More specifically, in the tests on the UR wall, the stiffness was set to approximately 4300 kN/m to represent the effect of a flexible timber floor. In the tests on the strengthened specimens, the system was stiffened to 7500 kN/m to account for the possible strengthening and stiffening of the floor (e.g., by bracing steel straps along the diagonals) and the improvement of its connection to the top of the wall. For this purpose, threaded bars were installed to connect the metal beams and reduce their clear span, and the rollers were injected with a 15 MPa compressive strength mortar.

To simulate the dead load of a roof, fifteen steel plates (for a combined weight of 15 kN) were placed on top of the wall and connected with threaded bars (Figure 1c, Figure 2a). Each bar was provided with an eyebolt and secured by steel ropes hanging from the crane bridge, to protect the shake table from the possible collapse of the top beam, as well as to ease the demolition of the specimen at the end of the tests.

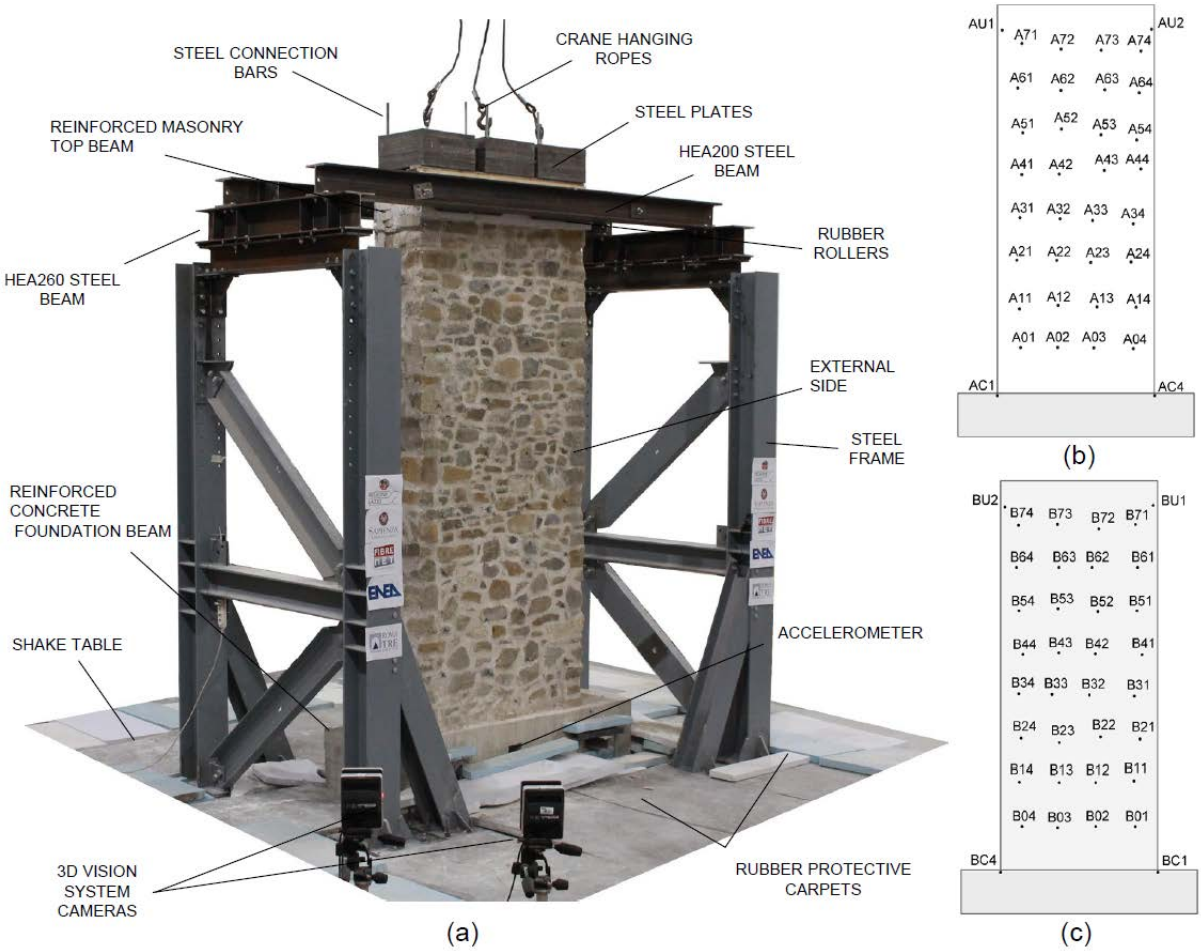

Figure 2. Experimental setup (a) and 3DVision retro-reflecting markers on the external (b) and internal (c) sides of the wall. ***Picture referred to CC wall.***

2.2.2 Shake table infrastructure

Tests were performed at ENEA Casaccia laboratory in Rome, Italy, equipped with a shake table with a 4 m × 4 m plan. The table is operated by four horizontal and four vertical actuators, has an operating frequency range of 0-50 Hz, an acceleration range of ± 3 g, a displacement range of ± 12.5 cm, and a maximum payload of 300 kN. The use of a shake table infrastructure allowed the application of acceleration time histories at the base of the specimens, thus reproducing the actual distribution of inertial forces experienced by the wall under earthquake base motion, including their dynamic amplification and rapid variation and reversal, which cannot be simulated in quasi-static tests [24]. Finally, the application of the vertical component of the seismic inputs made it possible to consider its effects on the dynamic response, which can be relevant on comparatively poor unreinforced masonry elements [25].

2.2.3 Instrumentation for displacement and acceleration measurement

A three-dimensional motion capture system, named 3DVision [26,27], was used to track the position of 78 retro-reflecting wireless passive markers by means of nine near-infrared high-definition digital cameras, at 200 Hz sampling frequency. As shown in Figure 2b-c, 4 markers were placed on the foundation, 68 on the wall specimen (34 on the external fair faced side and 34 on the internal plastered side), 4 on the top beam, and 2 on the steel transversal beam (note that the markers were glued on the stone units, so their position may slightly change from specimen to specimen). A three-axial accelerometer was placed on the foundation for an additional measure of the input, which was also used to calibrate the filtering parameters of the acceleration data.

2.3. Seismic inputs and experimental programme

Because the whole experimental programme was inspired by the damage caused on the built heritage during the 2016-2017 Central Italy earthquakes, and by the need of retrofitting the masonry buildings of that area, some records of that seismic sequence were used as inputs in shake table tests. More specifically, three record stations and three events were selected, namely Norcia, NRC (24 August 2016), Castelsantangelo sul Nera, CNE (26 October 2016), and Amatrice, AMT (30 October 2016). The record stations are located in three different regions, such as Umbria, Perugia (PG) for NRC, Marche, Macerata (MC) for CNE, and Lazio, Rieti (RI) for AMT, all severely struck by the earthquakes. The three earthquakes were all generated by fault-normal focal mechanisms.

As already mentioned, both the horizontal (H) and the vertical (V) components were applied. The former one was the East-West component of the record and was applied in the out of plane direction of the wall. Table 3 collects their main information and intensity measures, such as peak ground acceleration (PGA), velocity (PGV) and displacement (PGD), as well as Housner Intensity (HI), for the natural scale input accelerograms, in their corrected version available in the ITACA database [28]. On the one hand, using several records (from different events, stations and site conditions) delivered some variability to the seismic input, preventing the tests from being affected by the specific properties of a single base excitation. On the other hand, the selected accelerograms had similar intensity, to pursue a progressive damage occurrence. Finally, the selection of seismic inputs had to consider the maximum displacement capacity of the shake table, which limited the PGD of eligible records. For all the above considerations the selected accelerograms are not the most severe records of the seismic sequence [29].

The acceleration amplitudes of both H and V components were scaled by means of a scale factor (SF) starting from 0.2 and progressing with 0.2 steps. Once a set of strong motion tests (NRC, CNE, AMT) with the same SF was completed, a white noise (WHN) test was performed for dynamic identification, which had a nominal maximum acceleration of 0.05 g and a duration of 120 s (Table 3) and was applied only in the horizontal direction. Table A.1 lists all the shake table tests performed on the three walls. For each test, the record station and the SF are indicated, together with a label which summarises both of them, and which will be used hereinafter to refer to the tests.

Table 3. Accelerograms used in shake table tests and nominal intensity measures for SF=1 of horizontal (H) and vertical (V) components.

Record Id	Location	Soil type[a]	Event date, UTC time	PGA[b] H; V [g]	PGV[b] H; V [cm/s]	PGD[b] H; V [cm]	HI[c] H; V [cm]
NRC	Norcia (PG)	B	2016-08-24, 01:36	0.360; 0.215	29.8; 11.6	5.32; 3.04	106.9; 34.9
CNE	Castelsantangelo sul Nera (MC)	C	2016-10-26, 19:18	0.537; 0.397	23.1; 19.6	2.73; 3.01	79.6; 44.7
AMT	Amatrice (RI)	B	2016-10-30, 6:40	0.532; 0.324	37.9; 31.4	6.02; 4.42	90.7; 69.4
WHN	*White noise*	–	–	0.050; 0.000	3.5; 0.0	0.40; 0.00	16.7; 0.0

[a] Soil type according to [30].
[b] PGA, PGV, PGD: peak ground acceleration, velocity, displacement.
[c] Housner Intensity: as in [31]

Table 4. Nominal and wall recorded intensity measures, of horizontal (H) and vertical (V) components, for SF=0.6.

Nominal / Wall	Record Id	PGA H; V [g]	PGV H; V [cm/s]	PGD H; V [cm]	HI H; V [cm]
Nominal	NRC	0.216; 0.129	17.83; 6.93	3.29; 1.71	64.18; 20.96
	CNE	0.322; 0.238	13.82; 11.74	1.65; 1.84	47.48; 26.60
	AMT	0.319; 0.194	22.69; 18.81	3.78; 2.71	53.88; 41.67
CC	NRC	0.213; 0.201	10.23; 5.14	2.03; 0.49	46.58; 16.61
	CNE	0.316; 0.259	13.95; 8.24	1.48; 0.66	40.55; 20.12
	AMT	0.463; 0.244	17.92; 15.14	1.53; 1.39	43.29; 31.29
CR	NRC	0.263; 0.159	11.43; 5.34	2.02; 0.59	46.70; 17.18
	CNE	0.294; 0.246	13.58; 8.18	1.37; 0.67	39.54; 20.12
	AMT	0.386; 0.230	17.21; 15.87	1.38; 1.41	41.20; 31.59
UR	NRC	0.264; 0.174	11.36; 5.35	1.97; 0.52	46.16; 17.56
	CNE	0.300; 0.262	13.18; 8.22	1.28; 0.71	39.26; 20.21
	AMT	0.363; 0.216	16.86; 16.01	1.28; 1.35	40.18; 31.93

As inescapable, the nominal accelerograms given as input to the shake table are slightly modified by the latter. In order to evaluate how accurate the shake table was during the testing programme, previous intensity measures were computed for input record and for all the tested walls (Table 4). Tests for SF=0.6 were considered, because this is the largest scale factor applied for all walls and all records (Table A.1). As evident from Table 4, the shake table introduces some ground motion variability with the same nominal input delivering somewhat different intensity measures for different walls. Recorded acceleration amplitudes are faintly larger than nominal ones, while velocity measures are slightly smaller and displacements smaller, emphasising that the shake table tends to make the motion richer in higher frequencies. The integral measure of Housner Intensity, not anchored to a single peak value, highlights a maximum difference between input and output of about 25%. In the following labels derived from accelerometric station name will be used, but it is understood that the base accelerograms used in computations and figures are those recorded on the shake table.

3. WALL SPECIMENS AND EXPERIMENTAL PROGRAMME

3.1. Strengthening system with CFRP connectors

The strengthening solution with CFRP connectors included the following elements and required the following installation phases:

1) *Grout injections*. After completing the construction of the wall, 24 holes were drilled on the fair faced masonry (external side) and 3 holes were drilled on each of the lateral sides, for injections (Figure 3a, Figure 4a) [32,33]. Perforations were performed in mortar joints, had ∅ 20 mm and were approximately 250mm deep. After a first injection of water, an NHL premixed mortar was grouted, slowly moving the injection nozzle out from the bottom of the hole, from the base of the wall to its top. The wet mortar, continuously mixed, was conveyed by a low-pressure hand-operated pump. In total, about 1.3 kN of dry mortar mix was injected in the wall, corresponding to about 15% of its volume and 12% of its weight. The mechanical parameters of the injection grout are listed in Table 1.
2) *Drilling of the holes for CFRP connectors through the stone units of the fair faced side*. When the injection grout had cured for one week, 39 holes were drilled through the largest stone units of the

external face. Their average density was 6.4/m^2 but they were spaced about 50 cm in the central and in the lower portion of the wall and about 30 cm in the upper portion and along the vertical edges, where leaf separation was expected. Percussion diamond drills were used to perform the holes (a ∅ 8 mm drill bit was used for making a first hole, which was then enlarged with a ∅ 12 mm drill bit), in about 200 min including air blowing. The holes did not cross the entire wall thickness and did not disturb the internal side, were 450mm long and were inclined by 3-5° downwards.

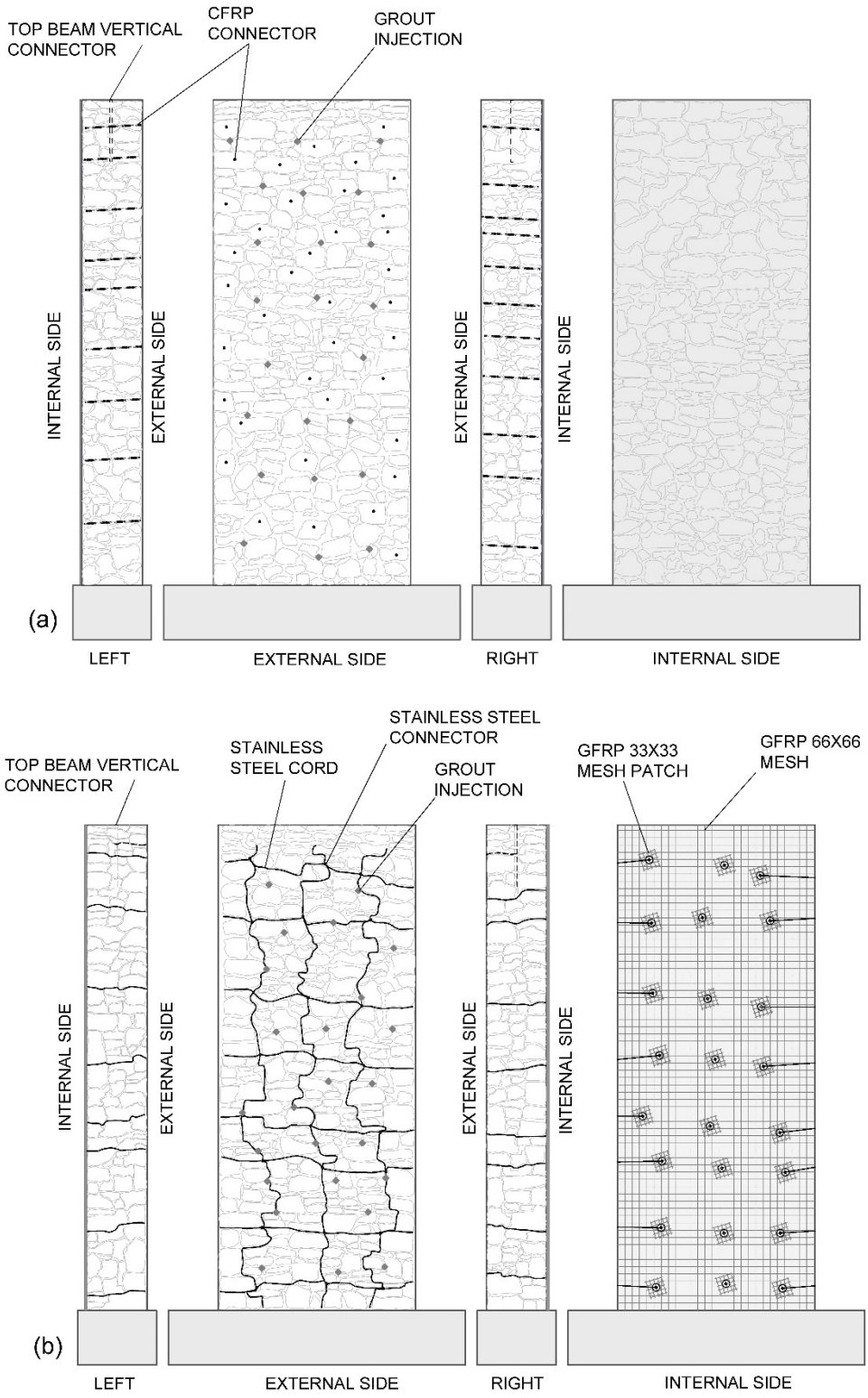

Figure 3. Layout of strengthening systems on CC (a) and CR (b) walls.

3) *Grouting in the holes of CFRP connectors*. A potassium-silicate primer was applied in the holes to consolidate the stones and the bedding mortar of the wall and promote a good bond of the injection grout (Figure 4b). This latter was a premixed cementitious mortar (see Table 1 for its mechanical properties) and was grouted in the holes with a handgun.

4) *Installation of the CFRP connectors*. While the grout was still fresh, CFRP bars (Figure 4c) were inserted in the holes (Figure 4d). Connectors had ∅ 6 mm and 420 mm length (mechanical properties are provided in Table 5). In order to improve their bond, their surface was sandblasted and they were dipped into the grouting mortar before insertion. Carbon was selected to manufacture the connectors to take advantage of its high tensile strength and stiffness while keeping their diameter (and, therefore, that of the holes required for their installation) as small as possible. The stone units of the fair faced side accommodating the connectors played the role of end plates, to provide a more effective engagement of the fair faced masonry leaf than that expected if the connectors were installed through the mortar joints, thus better contributing to prevent disintegration. Finally, the length of the CFRP bars ensured the connection between the front and the back leaves of the wall, with the aim of preventing leaf separation. It was estimated during installation that at least 50% of the CFRP bars, after crossing the inner core of the wall, reached a large stone unit of the back leaf (whose arrangement was hidden by the plaster), ensuring an effective connection. At the same time, the connectors did not fully cross the thickness of the wall, which left the internal side undisturbed. Therefore, in principle, this strengthening work could have been done without requiring to evacuate the building or suspend its use (at least provided that only the perimeter walls undergo strengthening works).
5) *Finishing*. The holes on the fair faced side were sealed with the injection grout to hide the heads of the connectors.

A number of studies investigated the idea of enhancing the seismic capacity of masonry structures working only from one side, either by externally bonded composites (see, amongst others, [10,34–38]) or through transversal connectors [39,40]. Most of these investigations, however, were devoted to in-plane shear or to monotonic out-of-plane bending. In the present case, instead, the specimen was subject to dynamic (inherently reversible) bending and multiple possible failure modes (flexure, leaf separation, masonry disintegration) needed to be prevented while preserving the fair face (so the use of externally bonded overlays on both sides or of connectors with end-plates was not feasible).

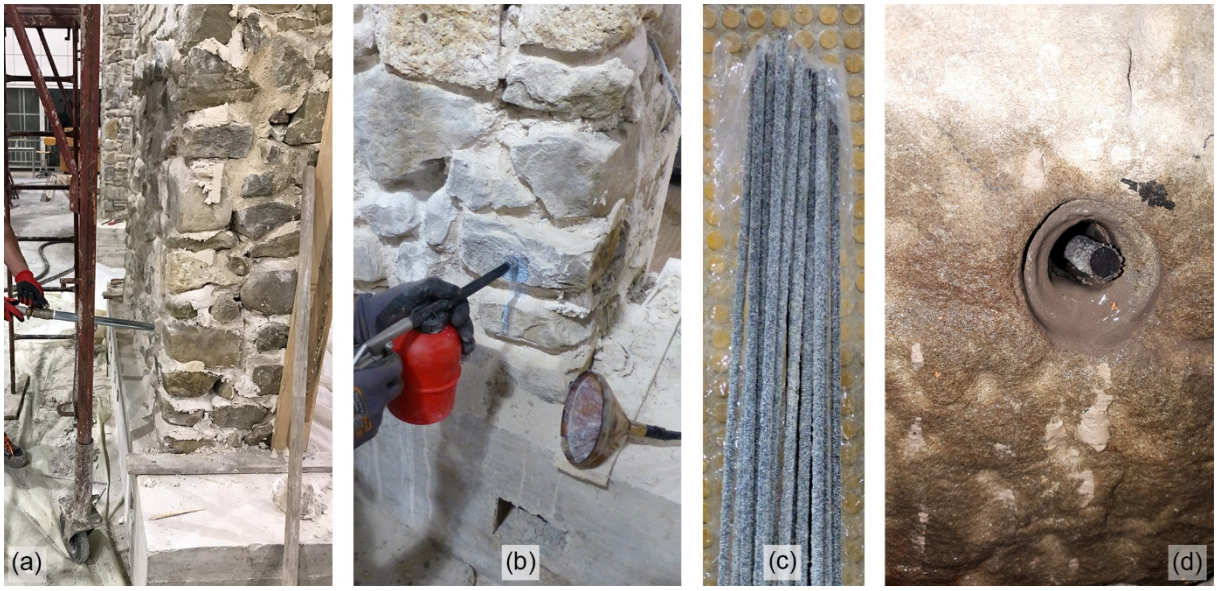

Figure 4. Phases of the strengthening works on CC wall: grouting (a) of injection mortar; injection of the primer (b); sandblasted connectors (c); end of CFRP connector in the grouted hole (d).

Table 5. Geometric and mechanical properties of the elements of the strengthening systems.
Average values. Coefficient of variation and number of tested specimens in round brackets.

Element of the strengthening system	A [mm^2]	E [GPa]	f_t [MPa]	ε_u [%]
CFRP connector	28.2	152.0	1840 (-; 3)	1.15
Steel connector	36.6	189.4	835 (1%; 10)	12.10
Steel wire	4.4	81.5	1340 (6%; 10)	2.58 (8%; 10)
GFRP mesh, vertical (warp)	11.6 (2%; 5)	25.0 (4%; 15)	494 (13%; 15)	1.98
GFRP mesh, horizontal (weft)	8.9 (11%; 5)	31.9 (2%; 15)	585 (9%; 15)	1.83

A: cross-section area. E: Young's modulus. f_t: tensile strength. ε_u: ultimate elongation.

3.2. Strengthening system with CRM and reinforced repointing of mortar joints

The strengthening solution investigated on CR wall was originally proposed by [41] and then tested by [42], but had never been validated before on a shake table. It combines two techniques, previously applied on both sides, such as CRM [22,43] and reinforced repointing connected by stainless-steel bars [44]. As for the integration of structural and energy properties, only few pilot studies, e.g., [45], have been carried out to date dealing with small masonry panels strengthened on both sides, but it has never explored for single-side applications to full-scale structural members. CR wall was strengthened by combining (i) the repointing of the mortar joints of the external side and their reinforcement with stainless-steel cords, (ii) the application of a thermo-insulating CRM overlay to the internal side, and (iii) the installation of stainless-steel connectors through the cross section of the wall. The works included the following phases.

1) *Grout injections*. The wall was injected with an NHL consolidating grout (the same used in CC wall) after completing the stonework. To this aim, 25 holes were drilled on the external face (Figure 3b) and 3 holes were drilled on each of the lateral sides of the specimen.
2) *Drilling of the holes and installation of stainless-steel connectors*. The original mortar was removed from the joints of the fair faced side (Figure 5a) and 24 ∅ 12 mm holes were drilled, starting from the bed joints (the stone units were not drilled), through the entire thickness of the wall (Figure 5b). In each hole, a ∅ 8mm threaded AISI316 (American Institute of Steel Industries) stainless-steel bar was inserted, which was provided with a ring welded at the end on the external side (the fair faced side, Figure 5c).
3) *Installation of stainless-steel cords in the mortar joints of the fair faced side*. Reinforced repointing was started on the external side (fair faced side) by placing AISI316 stainless-steel 49-strand-cords with ∅ 3 mm in the mortar joints, along the vertical and the horizontal directions, spaced about 500 mm. The horizontal and vertical cords crossed each other at the steel connectors and passed through their rings. The wire ends were anchored at the vertical connectors of the top beam, at the foundation, and at the back end of the connectors, passing over stainless steel L-shaped guides at the corners of the wall. The layout of the cords followed the joints (Figure 3b, Figure 5d), and was designed to maximise the distributed retaining effect against disintegration (which required short spacing) while minimizing the number of connectors for both costs and compatibility considerations. Indeed, it should be considered that the connectors are placed at every intersection between vertical and horizontal steel cords and that drilling the holes unavoidably entails some disturbance to the masonry (it may cause micro-cracking). The cross section of the cords was determined through simplified calculations in which the wall was considered as a simply supported beam under compression and bending [46].
4) *Laying of the GFRP mesh on the internal side*. The CRM overlay on the internal side was started by laying a GFRP mesh, with 66 mm × 66 mm grid spacing, over the entire surface of the wall, including the top beam (Figure 5e). Given the uneven surface of the stonework, no spacers were needed to leave clear space between the mesh and the substrate. At each threaded bar, a 150 mm × 150 mm patch of 33 mm × 33 mm GFRP mesh was added to spread the load, and a washer and a nut were placed to complete the connection (Figure 5f). Note that the original plaster should have been completely removed, if present, but, in this case, it was just decided to omit it at all.
5) *Tightening of the strengthening system*. The nuts were screwed in to tighten the steel cords and make them keep their position during the following phases, as well as to enhance the effectiveness of the connection between the steel cords on the external side and the GFRP mesh on the internal one.
6) *Repointing of the fair faced side joints*. The intervention on the external side was completed by repointing the joints (both those housing the steel cords and the other ones) using an NHL premixed mortar (whose mechanical properties are reported in Table 1) applied by a low-pressure nozzle (Figure

5g). This mortar enhanced the adhesion of the steel cords with the original substrate and made the strengthening system invisible, preserving the fair face.

7) *Application of the thermo-insulating mortar of the CRM on the internal side*. CRM was completed by spraying an NHL premixed mortar by means of a nozzle (pumping a mix of wet mortar and air stream) over the GFRP mesh (Figure 5h). The overall thickness of the CRM was about 30mm, which is similar to that of a typical plaster layer. At the same time, however, its formulation was developed to provide both a structural strengthening and a thermal insulation.

Figure 5. Phases of the strengthening works on CR wall: removal of the mortar from the joints of the external side (a); drilling of the holes for the connectors (b); stainless steel connector (c); stainless steel cords placed in the mortar joints (d); GFRP mesh laid over the internal side (e); nut-washer-patch at connector-mesh intersection (f); repointing of the mortar joints of the external side (g); machine application of the thermo-insulating mortar over the GFRP mesh of the internal side (h).

4. SHAKE TABLE TEST RESULTS

4.1. Damage development

As written before, the shake table tests were performed under natural accelerograms multiplied by a SF, starting from SF=0.2 and progressively increased by 0.2 steps. The UR specimen was badly damaged already during the test sequence with SF=0.6 and collapsed during CNE08 (CNE input record, SF=0.8) [11]. In the first tests, in which the intensity of the base excitation was relatively low (until SF=0.8), the strengthened walls, instead, remained basically elastic an no damage was observed. The very first small cracks in CC and CR walls appeared after AMT10, but some significant damage started developing only during the sequence with SF=1.2. This behaviour indicates the effectiveness of both strengthening solutions, which improved the seismic response of the wall and would have allowed it to sustain basically undamaged the natural scale records selected for this shake table investigation. The main damage sequence is shown in Figure 6, a detailed qualitative description is presented in Table A.1, and snapshots of the ultimate limit state are displayed in Figure 7.

As for the CC wall, one stone unit, just below the crowning beam, debonded from the surrounding ones and fell on the table during NRC14. Other stone units, next to it, fell down in the following tests (AMT14), both from the external side (Figure 7b) and from the internal side (Figure 7d), separating the wall from the top beam. Based on such damage state, ultimate limit state conditions were considered achieved.

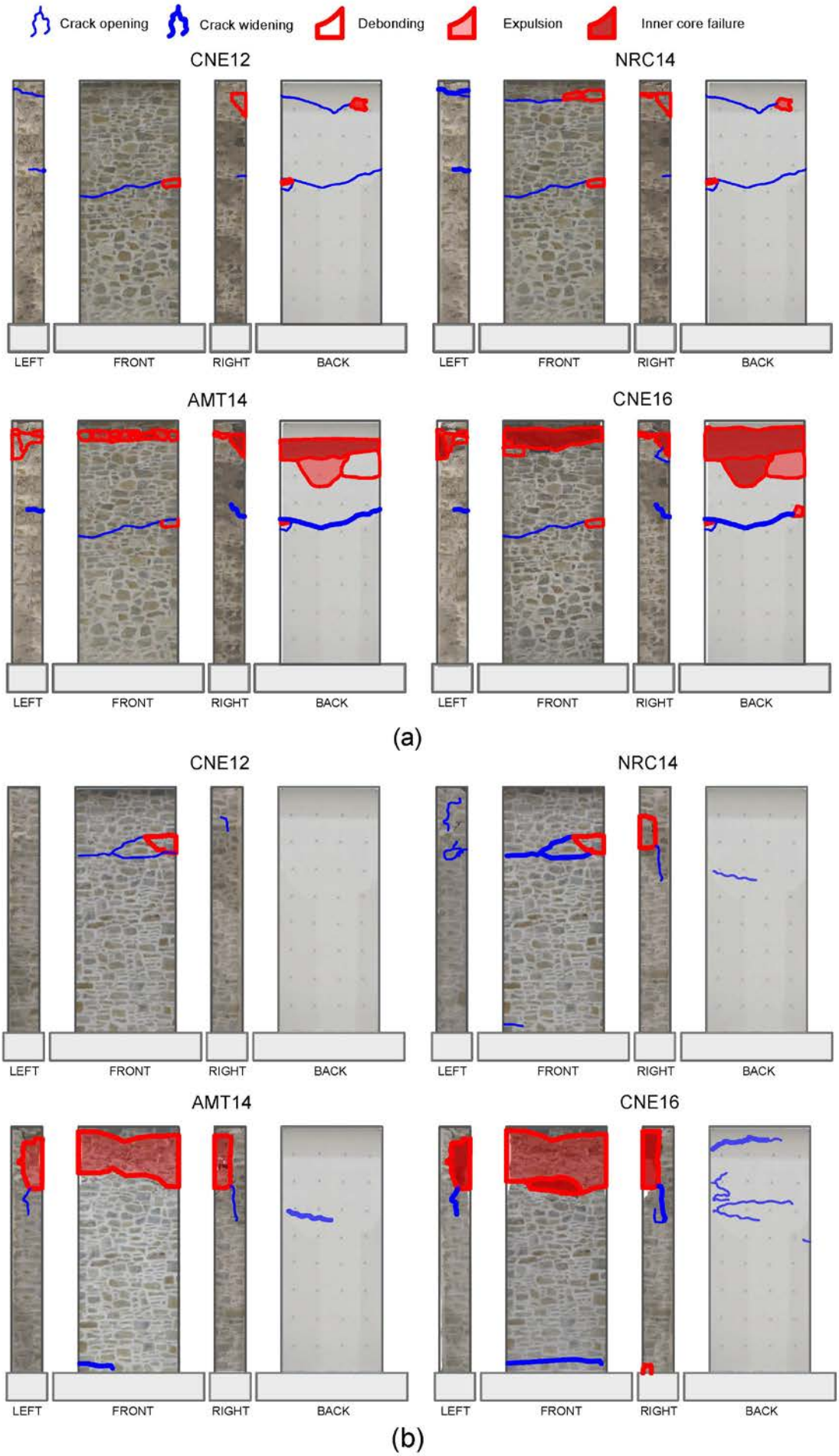

Figure 6. Damage development on CC (a) and CR (b) walls.

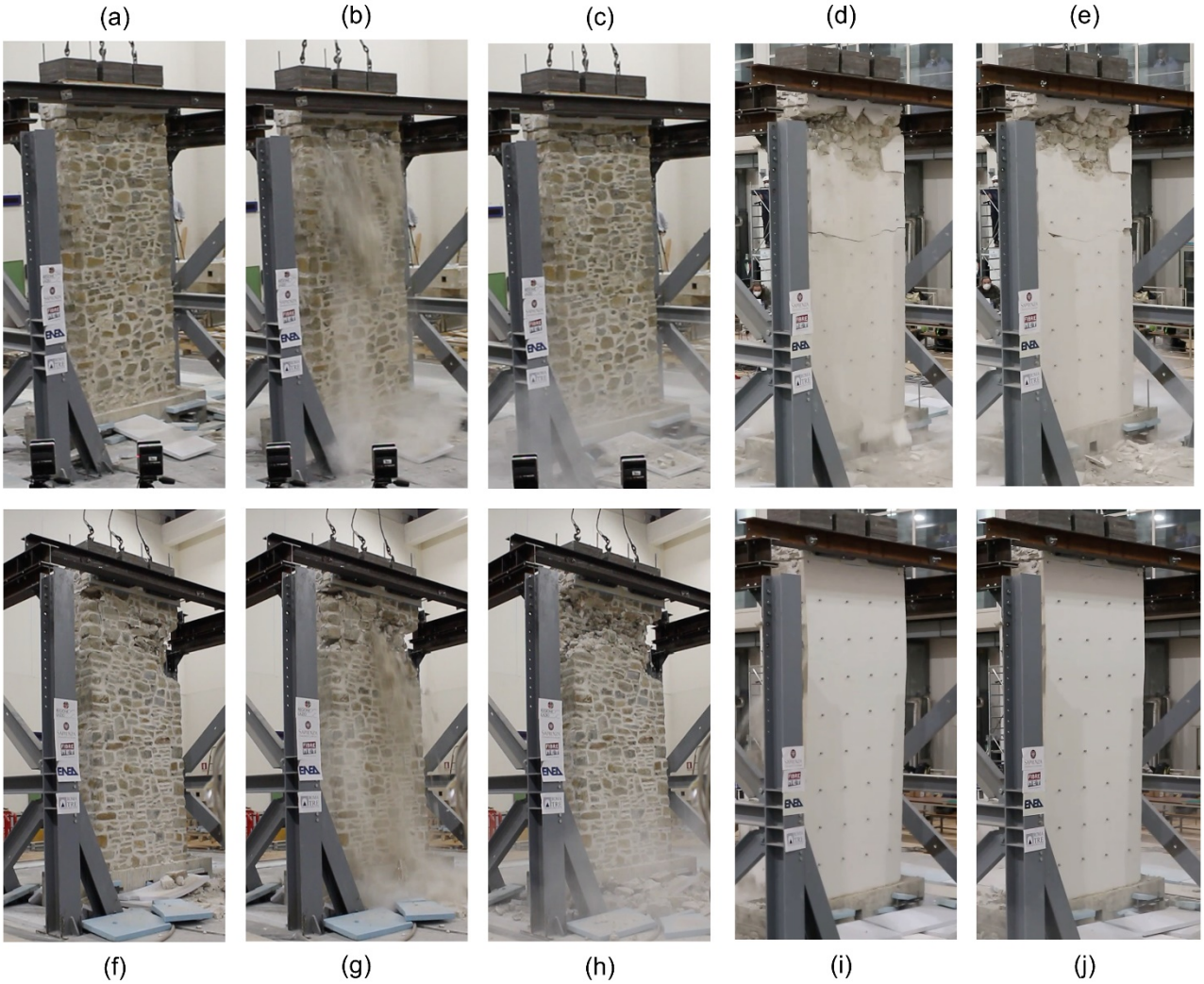

Figure 7. Ultimate limit state attainment during AMT14 tests. (a-e) CC wall, (f-j) CR wall; (a-c) and (f-h) external side, (d-e) and (i-j) internal side; (a) and (f) condition before the test, (b,d) and (g,i) maximum response, (e) and (j) condition after the test.

On the other hand, no clear sign of leaf separation or of masonry disintegration of the stonework (apart from the top of the wall) was detected (Figure 6a, Table A.1). The maximum absolute acceleration recorded at the base of the wall during AMT14 was 1.03 g. After AMT14, it was decided to perform a white noise test (WHNh) and two further strong motion tests with higher SF (NRC16 and CNE16), during which the wall behaved monolithically, rocking on its foundation, and its complete collapse took place due to the falling of several stone units.

As for CR wall, some stone units fell down during CNE14, moving the stainless-steel cords out of their original location, which slackened them, and compromised the effectiveness of the reinforcement in the repointed joints. This cord loosening, in its turn, triggered the disintegration, which further developed during the following test (AMT14), leading to the attainment of ultimate limit state conditions. More specifically, the fall down of the front leaf (Figure 7g) made the transversal connectors useless, whereas the back leaf (strengthened with CRM) exhibited a limited damage (Figure 6b, Table A.1, Figure 7j). The maximum absolute acceleration recorded during AMT14 was 0.99 g. Another white noise test (WHNh) and another strong motion test (NRC16) were performed, during which some stones from the inner core fell down and the cracks on the lateral sides and on the back side widened.

The comparison between the two crack patterns indicates that damage evolved similarly in CC and CR walls at least until the attainment of ultimate limit state conditions. The same areas of the specimens were involved, such as the stones in the upper portion of the external leaf (which exhibited the most severe damage) and the middle of the internal side (which exhibited a horizontal crack). On the other hand, some differences were observed. First, the internal side of the CR wall was less damaged, thanks to the presence of the CRM overlay, than that of the CC wall. As for this specimen, it should also be considered that the plaster on the internal side in real cases may be weaker than that applied in the laboratory, such that an even worse damage

might be expected, especially in historical structures. Finally, more cracks on the lateral sides (associated with leaf separation) developed in CR wall with respect to CC wall, showing the good effectiveness of the transversal connectors installed through the stone units.

4.2. Displacements

A quantitative evaluation of the seismic performance of the walls is provided by the displacements measured by the 3DVision system. The out of plane displacements (d) profiles are shown in Figure 8 under the same input record (CNE) at three SFs (0.6, 0.8 and 1.4). The profiles are represented for the time instant when the average displacement of the seventh row of markers from bottom attains its maximum. More specifically, for the onward displacements of the external side, the average of markers A61, A62, A63, and A64 (external side) is considered, whereas for the backward displacements of the internal side, the mean displacement of markers B61, B62, B63, and B64 is taken. Note that the seventh row of markers is not exactly at the same height for all the specimens, but is at about 2.50 m for CC wall, 2.68 m for CR wall, and 2.53 m for UR (height measured about the RC foundation).

The displacement profiles are linear for all the walls, highlighting a monolithic behaviour up to the development of significant damage and the onset of the collapse mechanism. As for the UR wall, this mechanism started during CNE06 (Figure 8a) and progressively evolved in the following tests. During CNE08, the last test before collapse, the maximum displacements were +53 mm for the external side (the fair faced side) and –25 mm for the internal side. At this stage, CC and CR walls were still elastic, with the maximum displacements of 5÷10 mm recorded at the top (Figure 8b). The development of cracks modified the deflection of both the strengthened specimens during the test sequence with SF=1.4. Figure 8c shows the profiles for CNE14, in which the maximum displacements were +36 mm / –23 mm for CC and +28 mm / –32 mm for CR.

Figure 9 shows the horizontal out of plane displacement time histories of the external and of the internal sides of the three walls, for the same tests of Figure 8. Markers A62 and B61 were selected for the external and internal sides, respectively, which provided complete measurements. Consistently with the profiles of Figure 8, UR wall displayed larger deflections than CC and CR (Figure 9a,b), and a residual value on the internal side, already at test CNE06 (Figure 9b). The displacements of UR diverged at collapse under CNE08 (Figure 9c,d), while those of CC and CR were still fully reversible. The responses of the strengthened walls remained similar also under stronger inputs, until the development of damage on the internal side of CC wall entailed larger peak and residual displacements with respect to CR, in which CRM limited irreversible phenomena at least for markers monitored in Figure 9f.

The horizontal out of plane displacement of the seventh row of markers on the external side of CC and CR walls (d_6) is plotted together with the vertical top displacement (u) in Figure 10. The out of plane deflection, be it positive (forward) or negative (backwards), always results associated with the uplift of the crowning beam. This outcome highlights that, for the out of plane mechanism to develop, it is necessary that the vertical displacements are free. On the other hand, if the uplift of the top of the wall is constrained, an arch effect arises in the wall, and the horizontal accelerations required to activate the failure mechanism are higher if compared with the case of unconstrained uplift [46–48]. Finally, this result confirms the opportunity of designing an experimental setup that represented the actual boundary conditions experienced by a masonry wall, in which a floor or a roof delivers additional compression but may hardly restrain vertical displacements.

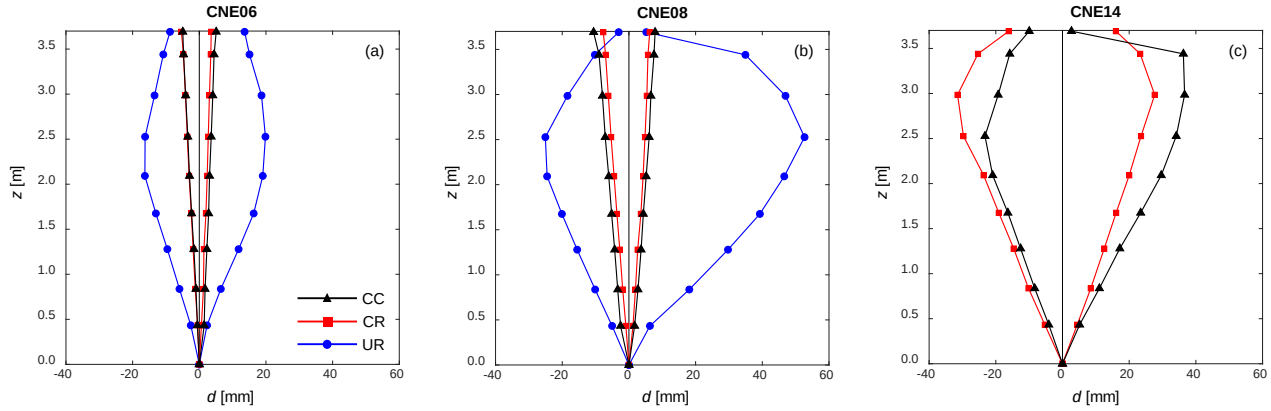

Figure 8. Out of plane displacement profiles under CNE06 (a), CNE08 (b) and CNE14 (c) seismic inputs.

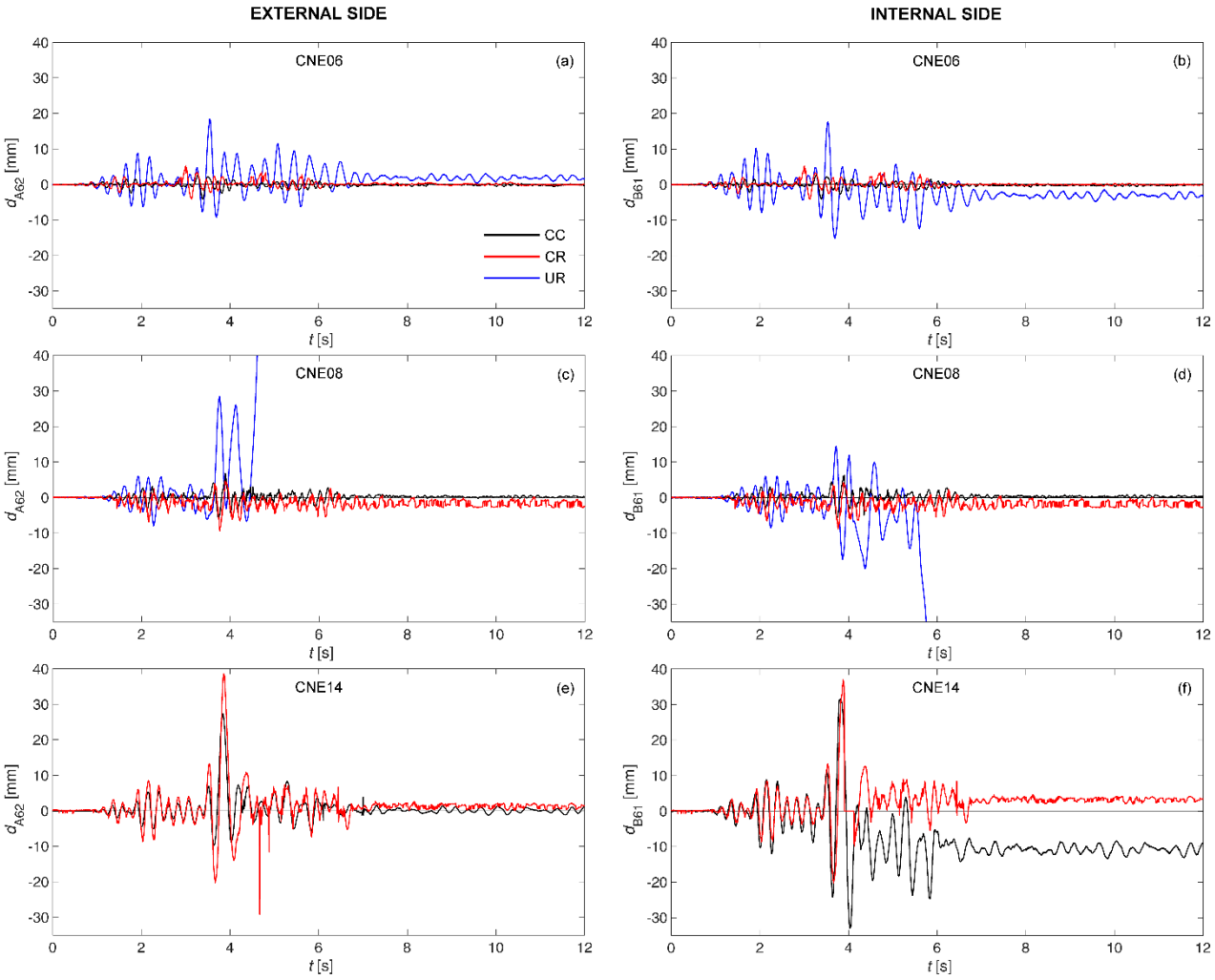

Figure 9. Out of plane displacement time histories of the external (a,c,e) and of the internal (b,d,f) sides for CNE06 (a,b), CNE08 (c,d) and CNE14 (e,f) tests.

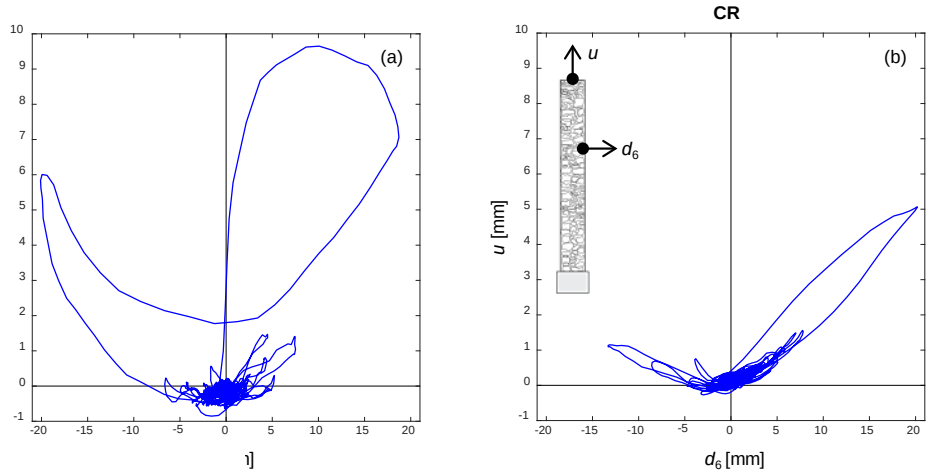

Figure 10. Vertical displacement of the top beam vs. horizontal out of plane displacement of the wall for CC(a) and CR (b) walls under AMT12 seismic input. ***Displacements are calculated from the average of the markers on the 7th row. Positive displacements refer to the external side (fair faced side) whereas negative displacements refer to the internal side.***

4.3. Leaf separation

As reported in [11], the damage and the collapse of the UR wall was ruled by the separation between the external and the internal leaves and by the disintegration of the masonry of the fair faced side. In order to investigate the effectiveness of the proposed strengthening techniques in preventing leaf separation, the relative displacement (δ) between some significant markers on the fair faced side (A41 and A61 near the left corner, and A44 and A64 near the right one) and the corresponding markers on the other side (B41, B61, B44, and B64) is plotted in Figure 11. The strong motion tests are shown in sequence, to identify when leaf separation occurred and detect the residual amplitude of the separation crack at the end of each test. An overall depiction of leaf separation at the end of some significant tests is delivered by the contour plots of Figure 12. The first 200 s (approximately until AMT04) were omitted in the plots, since no cracks developed in the initial tests of the test series.

CFRP connectors effectively prevented leaf separation along the entire shake table test series (Figure 12a), even in the last tests when collapse took place (note that the stones that fell down were above the markers represented in Figure 11a and that such collapse took place after the last test shown in Figure 12a, because 3DVision data were made unavailable by dust discharge and stone falling). On the other hand, some separation was detected on the left side of CR wall. The relative displacement A64−B64 attained 4 mm after AMT12, 21 mm after C14 and diverged during CNE14, indicating that the stone where the marker was glued fell down. Smaller, but not negligible, displacements were recorded also for A61−B61 after NRC14 (5 mm) (Figure 11b). The contour plots show that leaf separation was still localised until AMT12 and progressively extended to the entire upper portion of the wall after NRC14 and CNE14 (Figure 12b), when the slackening of the steel cords in the repointed joints (caused, in its turn, by the falling of the stones) compromised the effectiveness of the system.

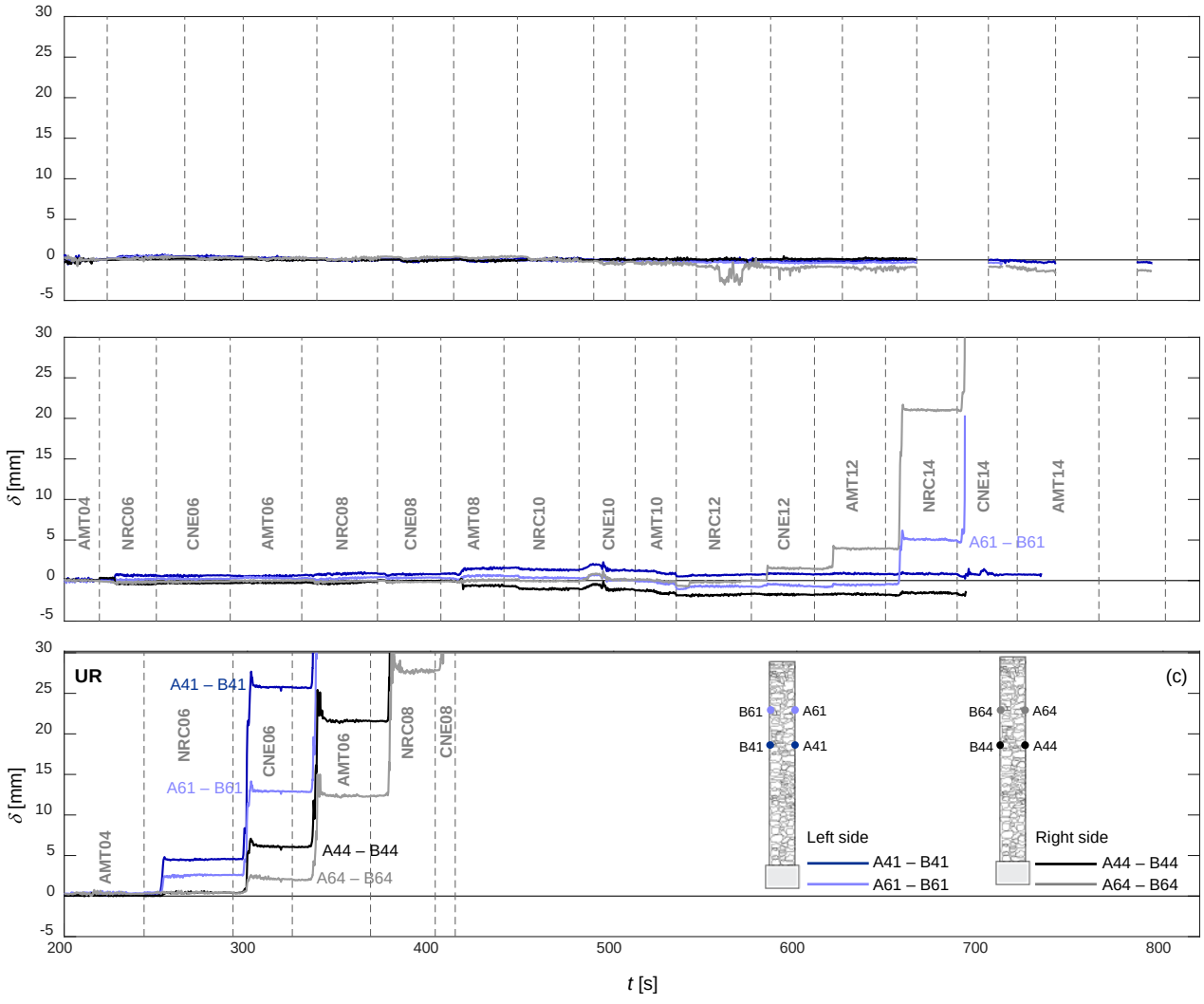

Figure 11. Relative displacements between the two leaves of CC (a), CR (b) and UR (c) walls.

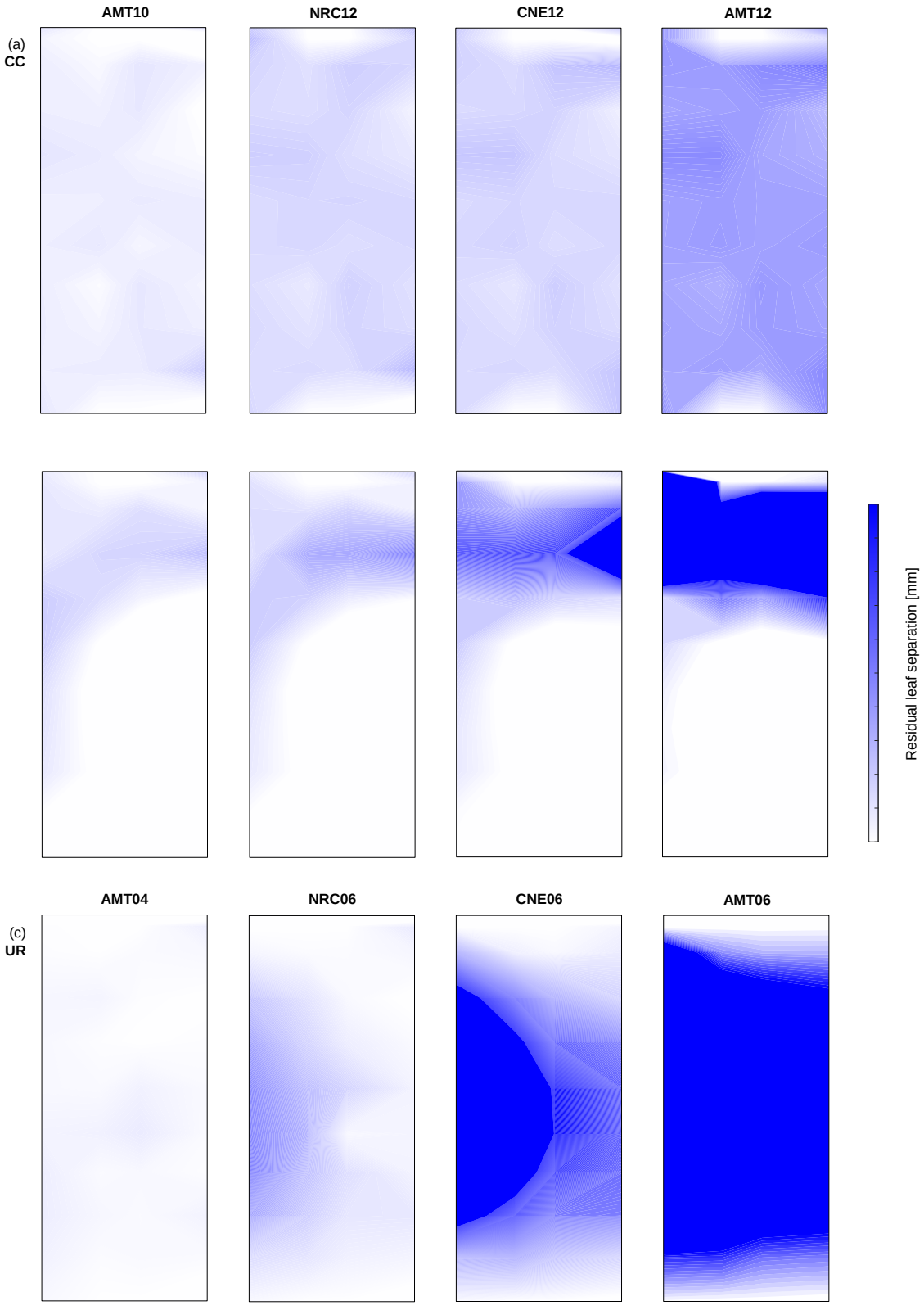

Figure 12. Residual leaf separation CC (a), CR (b) and UR (c) walls at the end of the most significant tests.

The effectiveness of the two strengthening techniques is highlighted by the higher relative displacements measured near the corners of UR specimen, as well as by the larger portion of this latter exhibiting leaf separation, which first concentrated on the left side, from NRC06 (see A41–B41 and A61–B61 in Figure 11c and the contour plot in Figure 12c) and then extended after CNE06, up to involving the entire width of the wall after AMT06 (see A44–B44 and A64–B64 in Figure 11c and the contour plot in Figure 12c).

4.4. Seismic capacity

The overall seismic response of the walls tested on the shake table is presented in Figure 13 in terms of base acceleration versus out of plane displacement curves. The maximum positive value ($a_{h,max}$) and the minimum negative value ($a_{h,min}$) of the horizontal acceleration time histories at the base of the wall are on the *y*-axis. They were measured by the accelerometer placed on the RC foundation (Figure 2, a 4th order band-pass Butterworth filter at 0.2÷25 Hz and a 2nd order baseline correction were applied). The maximum average displacement (d_A) of the four markers on the 7th row on the external side (A61, A62, A63, A64) and the minimum average displacement (d_B) of the corresponding four markers on the internal side (B61, B62, B63, B64) are on the *x*-axis. Each plot corresponds to one input record (NRC, CNE and AMT) and compares the seismic response of the three walls (CC, CR and UR).

The relationship between base accelerations and out of plane displacements is basically linear for low-intensity inputs, and no clear difference of stiffness is detected. Then, the development of damage is associated with a reduction of the slope of the curves, which occurs at higher accelerations for CC and CR with respect to UR, consistently with the evolution of damage described above. Non-negligible differences of base accelerations and displacements, stiffness and shape of the curves result from the different characteristics of the selected input records.

The maximum absolute horizontal accelerations recorded at the base of the three walls are 1.03 g for CC, 0.99 g for CR and 0.45 g for UR. Assuming this value as an indicator of the seismic capacity of the wall, the improvement with respect to UR was 127% in the case of CC and 120% in the case of CR. On the other hand, no significant change of the maximum displacements was found, as shown by the curves plotted in Figure 13, which refer to the 7th row of markers. Analogous conclusion can be derived from the displacements recorded by the other markers, which are not shown for the sake of brevity. Nevertheless, the displacements attained by UR wall were irreversible and mainly associated with cracking and stone sliding and dislocation, whereas those exhibited by CC and CR walls were mainly associated with their dynamic response and, therefore, largely reversible, thus indicating that the strengthening systems also provided an upgrade of displacement capacity.

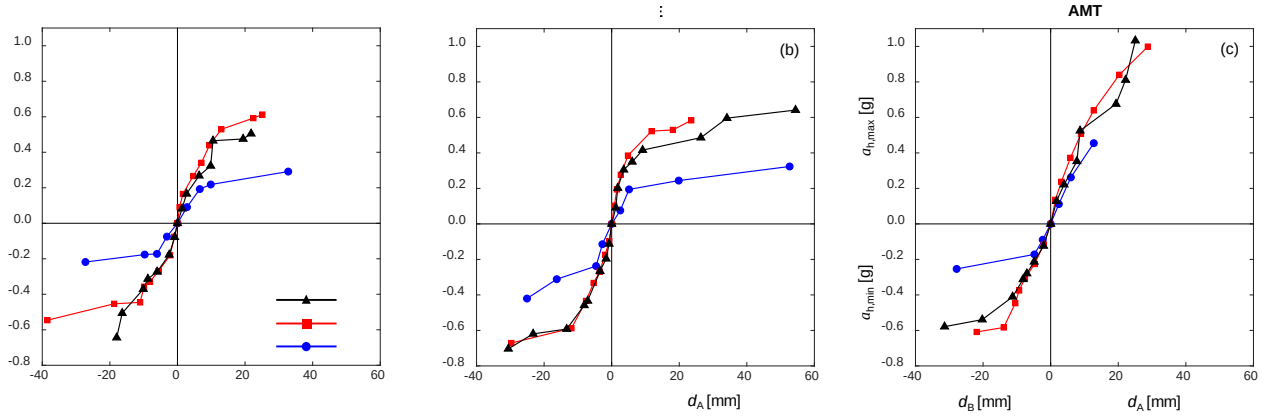

Figure 13. Maximum and minimum base accelerations vs. out of plane maximum displacements under NRC (a), CNE (b) and AMT (c) seismic inputs. ***Displacements are calculated from the average of the markers on the 7th row. Positive displacements refer to the external side (fair faced) whereas negative displacements refer to the internal side (plastered).***

4.5. Dynamic properties

The fundamental out of plane frequency of the wall (*f*) was calculated with a multiple-input-multiple-output approach [49]. The four markers on the RC foundation were considered for the seismic input and the top 48 markers on the wall (from the 3rd to the 8th row) were taken for the output. Acceleration time histories were obtained by double derivation of marker displacements and no filter was applied. The 192 transfer functions calculated for each output-input couple of markers were averaged to derive information on the overall dynamic properties of the specimens. The resulting frequencies are shown in Figure 14 for the three walls under all the strong motion and white noise tests. The mean frequencies for the three tests with the same SF were also calculated (and are plotted with the dotted line in the graph).

CC and CR confirm their similarity. They both exhibited an initial frequency of about 7 Hz, which progressively decreased to 4.5 Hz in the test sequence with SF=1.2, and the frequency near collapse was about

3 Hz for both the walls. Random vibrations (hollow dots) present higher values compared to earthquake ground motion tests (filled dots). This feature is probably the effect of a non-linear, amplitude-dependent behaviour.

On the other hand, the lower values of the UR specimen can be explained by the different stiffness of the top restraint. Indeed, the frequency increase after Test #04 (from 5.2 Hz to 5.9 Hz) was related to a modification of the top boundary [11], delivering a value close to those of the strengthened walls, especially in white noise tests. The comparison of the frequencies of CC and CR walls with those of UR indicates that the strengthening systems did not significantly increase the stiffness of the wall in the undamaged state, but effectively limited progressive damage accumulation under repeated earthquake base excitations.

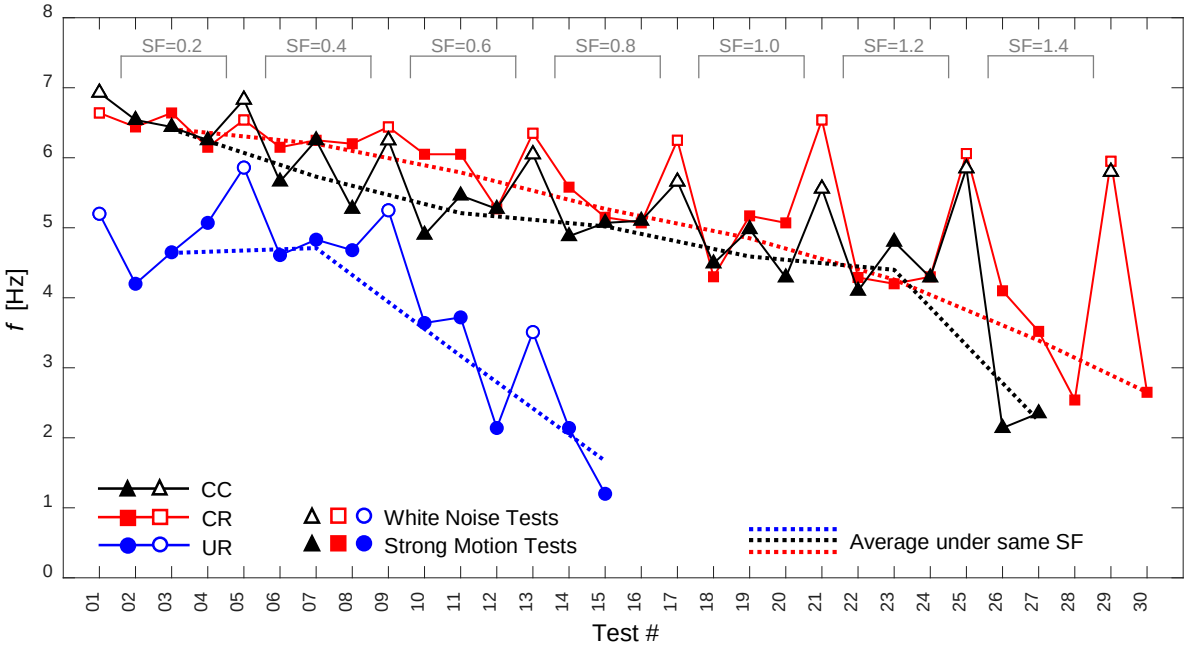

Figure 14. Fundamental frequency of CC, CR and UR walls during the shake table test sequences.

5. PRELIMINARY REMARKS ON DESIGN CRITERIA

The present shake table investigation is insufficient, by itself, to derive comprehensive information for the design of the proposed strengthening techniques. Nonetheless, the organization of the experiments, the selection of materials and the design of the strengthening systems and their execution, as well as the analysis of test outcomes provided some preliminary indications, which may be useful for the implementation in rehabilitation practice.

Concerning non-crossing connectors installed through the stone units of the façade (CC wall), which is a completely new strengthening method, the main design parameters are the tensile and pull-out strength of the connectors and their spacing. The use of carbon or steel connectors allows minimizing their size and, therefore, the disturbance caused by hole drilling as well as the visual impact, while ensuring sufficient strength for contrasting leaf separation. Glass and basalt connectors are cheaper, but larger sections may be needed. Connector surface roughness and proper installation are crucial for the development of adhesion with the stone units, which may result more critical than tensile failure. Laboratory or field pull-out tests appear necessary to derive quantitative information for the masonry, connectors and grouting matrix (be it mortar or resin) in question. Finally, spacing depends on the possible occurrence of disintegration. Walls with small stones, weak mortar and irregular arrangement, due to their higher vulnerability against disintegration, may require closer connectors than walls with large units laid regularly with a stronger mortar. It should however be considered that for extremely weak walls, a suitable enhancement of seismic capacity may result unachievable with this technique.

As for external mortar joint repointing by means of stainless-steel cords combined with internal CRM overlay (CR wall), despite some tests have been already performed by other authors [41,42], design guidelines have not been developed yet. In this case, the main parameters are the spacing of the steel cords and the strength per unit width of the FRP mesh embedded in the CRM. Reinforced repointing is intended to contrast masonry disintegration and enhance out-of-plane bending strength. Since the diameter of the cords should be kept small

(3÷5 mm) to limit stiffness and to ease installation, the effectiveness of the intervention depends on cord spacing, which needs to be smaller as walls tend to be more prone to disintegration. Steel cords also enhance out-of-plane bending strength, and the design relations developed for FRCM [46] could well be adapted for computations. CRM proved effective to avoid masonry disintegration on its side and specific design is unneeded. As for the out-of-plane bending capacity, the required strength per unit of the FRP mesh can be determined with the design method of FRCM. For this purpose, the thickness of the mortar layer can conservatively be neglected, only attributing it the role of ensuring (with the connectors) stress transfer between the substrate and the FRP mesh. Finally, transversal connectors prevent leaf separation and, as long as stainless-steel bars are used, they are not the crucial element for the ultimate capacity of the strengthened wall, because their tensile and pull-out failures appear unlikely. In principle, their spacing may be larger than that of the CFRP connectors discussed above, and it is rather ruled by the spacing of the cords in the repointed joints.

CONCLUSIONS

Shake table tests on full scale specimens demonstrated the effectiveness of two low-impact techniques for the seismic strengthening of rubble masonry walls. The investigated strengthening systems make use of either CFRP connectors installed from outside through the stone units leaving the internal wall surface undisturbed (CC wall), or of reinforced repointing of the mortar joints of the fair faced side and of a CRM overlay on the internal side, connected by stainless steel bars (CR wall). Grout injections were also performed to fill the voids and improve the mechanical properties of the masonry. Both the strengthening systems significantly enhanced the out of plane seismic capacity of the walls under earthquake base excitation with respect to the unstrengthened reference specimen (UR wall) tested first. More specifically:

- wall leaf separation was effectively constrained by the transversal connectors, even when not crossing the entire wall thickness, as in CC wall; masonry disintegration, was significantly delayed by the installation of the connectors through the stone units (CC) or by the reinforced repointing of and the transversal connectors through mortar joints;
- progressive damage accumulation under repeated seismic inputs was considerably limited, as demonstrated by the crack pattern surveyed during test execution, the crack width and leaf separation measured by means of the 3DVision tracking system over the entire wall surface, and the fundamental frequency calculated by a multiple-input-multiple-output experimental modal analysis approach;
- strengthening systems increased the stiffness of the walls by only 20% (but the effects of grout injections and slightly different top restraint should also be considered);
- accelerations recorded at the base of the walls associated with the occurrence of the first damage increased from 0.22 g (UR) to 0.59 g (+168%, CC) and 0.58 g (+163%, CR);
- in CC specimen, collapse took place when the stone units of the fair faced side, immediately below the crowning beam, fell down and caused the progressive separation of the wall from the crowning beam;
- in CR specimen, some stone units fell down from the external side of the wall, which moved the stainless-steel cords out from their original location, slackening them and compromising their effectiveness, which in its turn, triggered the disintegration;
- displacement capacity (out of plane deflections at collapse) remained basically unchanged (but collapse was attained under much more intense seismic input in strengthened walls);
- maximum absolute base acceleration increased from 0.45 g (UR) to 1.03 g (+127%, CC) and 0.99 g (+120%, CR); scale factors (SF) achieved in the tests on strengthened walls (SF=1.4 at ultimate limit state conditions) indicated that they could have overcome the natural scale records selected for the shake table investigation basically undamaged.

The strengthening systems investigated in this study not only proved effective, but also entail low impact and sustainability from multiple standpoints:

- they both preserve the fair faced masonry of the fair faced side, thus allowing its architectural value to be kept consistent with pre-existing state and urban context;
- they both make use of lime-based mortars for repointing, which ensure the physical-chemical compatibility with original substrate materials (only the CC connectors were grouted with a cement mortar in this investigation);
- the materials (stainless steel, alkali-resistant glass fibres, carbon fibres) ensure durability and, therefore, the effectiveness of the strengthening intervention and the safety level of the strengthened wall in the long-term;

- in the CC system, CFRP connectors are installed from outside and do not perforate the entire wall thickness, thus leaving the internal side of the wall undisturbed. Therefore, in principle, this strengthening work can be done (i) without evacuating the building or suspending its use (provided that working only on the perimeter walls is sufficient) and (ii) safeguarding a decorated side of the wall (by implementing the intervention from the opposite one);
- in the CR system, which required working on both wall sides, the CRM overlay entails the laying of a thermo-insulating mortar, thus providing both a structural enhancement and an improvement of the energy performances of the building.

On the one hand, the stone units (collected from buildings collapsed in an historical hamlet), the bedding mortar (formulated based on collected samples) and the bond pattern (designed from surveyed constructions), as well as the seismic inputs used in the tests, were selected to represent relevant conditions experienced by the built heritage struck by the 2016-2017 Central Italy earthquakes. On the other hand, despite the inherent variability of masonry constituents and construction practices, the abovementioned results can well be extended to rubble stone masonry structures in many countries in Europe and worldwide. For the same reason, from a design standpoint, engineering judgement still remains necessary to decide upon the density of connectors and the stone units to drill for inserting them, as well as to identify the layout of the stainless-steel cords and their spacing in reinforced repointing, based on (amongst others) stone size and arrangement, mechanical properties and conservation state of the bedding mortar, wall thickness and presence of bondstones across its section. With respect to this, it should be considered that the strengthening solutions proposed in this work might result unsuitable for masonry buildings presenting a prevalence of very small-size units, for which a significant upgrade of the seismic capacity is probably achievable only with reinforced overlays (e.g., FRCM, CRM) applied to the entire surface of both the internal and the external wall sides.

Finally, some features of the strengthening systems will need to be engineered to optimise construction phases and to reduce costs, for example:

- it is possible to envisage the use of a high-velocity, no-percussion, ∅ 12 mm drill mill, to perform the holes for the connectors, especially in the CC system in which stone units are drilled, to minimise the disturbance caused by vibrations. A shorter drill may be used at the beginning to avoid buckling, whereas a longer one may be used to reach the desired depth;
- in CR system, which entails drilling holes in the joints of the fair faced sides, the same set of drilled holes may be used for both grout injections and installation of connectors, to reduce costs and duration of strengthening works. This procedure appears unfeasible in CC system, in which drilling the stone units may require that the wall has already been rehabilitated;
- the details and the materials of the components of the strengthening systems may be modified, while keeping the mechanical principles at the basis of their effectiveness. For example, the FRP mesh of the CRM overlay may have different spacing or may be produced with carbon fibres in lieu of glass ones; the FRP connectors may be manufactured with glass or basalt fibres instead of carbon, and their surface may be ribbed instead of sandblasted, or they may be in galvanised or stainless steel, with ribbed or threaded surface; the cross section of the connectors may be round or squared; finally, the holes may be injected with a geopolymer mortar (instead of cement one) or with resin.

Despite these issues related to the implementation at the construction site, the strengthening techniques validated in this shake table investigation already appear promising for real-field applications, especially for fair faced rubble masonry walls, whose strengthening poses challenging difficulties. This investigation emphasises that traditional and innovative materials can be successfully integrated for safeguarding the built heritage in earthquake prone areas, with the additional advantage of combining structural effectiveness, low impact and conservation.

ACKNOWLEDGEMENTS

This work was carried out within the Research Projects “SICURA Sustainable technologies for the seismic protection of the cultural heritage” (2018-2020) and “SISMI Technologies for the safety improvement and the reconstruction of historical centres in seismic prone areas” (2018-2019) funded by Lazio Region. Fibre Net SpA (Pavia di Udine, UD, Italy) is kindly acknowledged for providing reinforcement materials and technical advice. UniCalce SpA (Lecco, Italy) provided the bedding mortar for the construction of the wall specimens. The intermunicipal operative office of Accumoli and Amatrice is kindly acknowledged for allowing the collection of the stone units from the hamlet of Collespada. SDS, GdF, FG and MS acknowledge funding from the Italian Ministry of Education, University and Research (MIUR), in the frame of the Departments of Excellence Initiative 2018-2022, attributed to the Department of Engineering of Roma Tre University. OA, LS and DM partially carried out this work under the program ‘‘Dipartimento di Protezione

Civile – Consorzio RELUIS''. The opinions expressed in this publication are those of the authors and are not necessarily endorsed by the Dipartimento della Protezione Civile.

DECLARATION OF COMPETING INTEREST

The authors declare that there is no known competing financial interests or personal relationships that could have appeared to influence the work reported in this paper.

CREDIT AUTHORSHIP CONTRIBUTION STATEMENT

Stefano De Santis: Conceptualization, Methodology, Supervision, Validation, Formal analysis, Investigation, Data Curation, Writing – original Draft, Visualization. **Omar AlShawa**: Conceptualization, Methodology, Formal analysis, Investigation, Data Curation, Visualization. **Gianmarco de Felice**: Conceptualization, Methodology, Supervision, Project coordination, Writing – review & editing. **Francesca Gobbin**: Conceptualization, Methodology, Formal analysis, Data Curation, Visualization. **Ivan Roselli**: Formal analysis, Data Curation. **Marialuigia Sangirardi**: Conceptualization, Methodology, Formal analysis, Data Curation, Visualization. **Luigi Sorrentino**: Conceptualization, Methodology, Supervision, Investigation, Data Curation, Writing – original Draft, Visualization. **Domenico Liberatore**: Conceptualization, Methodology, Supervision, Project coordination, Writing – review & editing.

REFERENCES

[1] D.F. D'Ayala, S. Paganoni, Assessment and analysis of damage in L'Aquila historic city centre after 6th April 2009, Bull. Earthq. Eng. 9 (2011) 81–104. doi:10.1007/s10518-010-9224-4.

[2] L. Sorrentino, S. Cattari, F. da Porto, G. Magenes, A. Penna, Seismic behaviour of ordinary masonry buildings during the 2016 central Italy earthquakes, Bull. Earthq. Eng. 17 (2019) 5583–5607. doi:10.1007/s10518-018-0370-4.

[3] A. Borri, M. Corradi, G. Castori, R. Sisti, A. De Maria, Analysis of the collapse mechanisms of medieval churches struck by the 2016 Umbrian earthquake, Int. J. Archit. Herit. 13 (2019) 215–228. doi:10.1080/15583058.2018.1431731.

[4] A. Rezaie, M. Godio, K. Beyer, Experimental investigation of strength, stiffness and drift capacity of rubble stone masonry walls, Constr. Build. Mater. 251 (2020) 118972. doi:10.1016/j.conbuildmat.2020.118972.

[5] G. Vlachakis, E. Vlachaki, P.B. Lourenço, Learning from failure: Damage and failure of masonry structures, after the 2017 Lesvos earthquake (Greece), Eng. Fail. Anal. 117 (2020) 104803. doi:10.1016/j.engfailanal.2020.104803.

[6] G. de Felice, S. De Santis, P.B. Lourenço, N. Mendes, Methods and Challenges for the Seismic Assessment of Historic Masonry Structures, Int. J. Archit. Herit. 11 (2017) 143–160. doi:10.1080/15583058.2016.1238976.

[7] L. Sorrentino, D. D'Ayala, G. de Felice, M.C. Griffith, S. Lagomarsino, G. Magenes, Review of Out-of-Plane Seismic Assessment Techniques Applied To Existing Masonry Buildings, Int. J. Archit. Herit. 11 (2017) 2–21. doi:10.1080/15583058.2016.1237586.

[8] C. Papanicolaou, T. Triantafillou, M. Lekka, Externally bonded grids as strengthening and seismic retrofitting materials of masonry panels, Constr. Build. Mater. 25 (2011) 504–514. doi:10.1016/j.conbuildmat.2010.07.018.

[9] F.A. Kariou, S.P. Triantafyllou, D.A. Bournas, L.N. Koutas, Out-of-plane response of masonry walls strengthened using textile-mortar system, Constr. Build. Mater. 165 (2018) 769–781. doi:10.1016/j.conbuildmat.2018.01.026.

[10] S. De Santis, G. de Felice, G.L. Di Noia, P. Meriggi, M. Volpe, Shake Table Tests on a Masonry Structure Retrofitted with Composite Reinforced Mortar, Key Eng. Mater. 817 (2019) 342–349. doi:10.4028/www.scientific.net/KEM.817.342.

[11] G. de Felice, D. Liberatore, S. De Santis, F. Gobbin, I. Roselli, M. Sangirardi, O. AlShawa, L. Sorrentino, Seismic behaviour of rubble masonry: shake table test and numerical modelling, Earthq. Eng. Struct. Dyn. (2021) submitted.

[12] O. AlShawa, G. De Canio, G. de Felice, S. De Santis, S. Forliti, D. Liberatore, D. Mirabile Gattia, S. Perobelli, F. Persia, G. Roselli, L. Sorrentino, Investigation of rubble-masonry wall construction practice in Latium, Central Italy, in: 12th Int. Conf. Struct. Anal. Hist. Constr. Barcelona 29 Sept. - 1 Oct., 2021.

[13] M. Giaretton, M. Valluzzi, N. Mazzon, C. Modena, Out-of-plane shake-table test of strengthened multi-leaf stone masonry walls, Bull. Earthq. Eng. (2017) 1–19. doi:10.1007/s10518-017-0125-7.

[14] EN 1015-11, Methods of Test for Mortar for Masonry. Part 11: Determination of Flexural and Compressive Strength of Hardened Mortar, European Committee for Standardization, Brussels, 2019.

[15] EN-12372, Natural stone test methods - Determination of flexural strength under concentrated load, European Committee for Standardization, Brussels, 2006.

[16] EN-1926, Natural stone test methods - Determination of uniaxial compressive strength, European Committee for

Standardization, Brussels, 2006.
[17] G. Roselli, D. Mirabile Gattia, O. AlShawa, P. Cinaglia, G. Di Girolami, C. Francola, F. Persia, E. Petrucci, R. Piloni, F. Scognamiglio, L. Sorrentino, S. Zamponi, D. Liberatore, Mortar analysis of historic buildings damaged by recent earthquakes in Italy, Eur. Phys. J. Plus. 134 (2019) 540. doi:10.1140/epjp/i2019-13024-2.
[18] K. Doherty, M.C. Griffith, N. Lam, J. Wilson, Displacement-based seismic analysis for out-of-plane bending of unreinforced masonry walls, Earthq. Eng. Struct. Dyn. 31 (2002) 833–850. doi:10.1002/eqe.126.
[19] H. Derakhshan, M.C. Griffith, J.M. Ingham, Out-of-Plane Behavior of One-Way Spanning Unreinforced Masonry Walls, J. Eng. Mech. 139 (2013) 409–417. doi:10.1061/(ASCE)EM.1943-7889.0000347.
[20] F. Graziotti, U. Tomassetti, A. Penna, G. Magenes, Out-of-plane shaking table tests on URM single leaf and cavity walls, Eng. Struct. 125 (2016) 455–470. doi:10.1016/j.engstruct.2016.07.011.
[21] D. Dizhur, M. Giaretton, I. Giongo, J. Ingham, Seismic retrofit of masonry walls using timber strong-backs, Struct. Eng. Soc. J. - SESOC. 30 (2017).
[22] S. De Santis, G. De Canio, G. de Felice, P. Meriggi, I. Roselli, Out-of-plane seismic retrofitting of masonry walls with Textile Reinforced Mortar composites, Bull. Earthq. Eng. 17 (2019) 6265–6300. doi:10.1007/s10518-019-00701-5.
[23] L. Giresini, M. Sassu, L. Sorrentino, In situ free-vibration tests on unrestrained and restrained rocking masonry walls, Earthq. Eng. Struct. Dyn. 47 (2018) 3006–3025. doi:10.1002/eqe.3119.
[24] A.A. Costa, A. Arêde, A. Campos Costa, A. Penna, A. Costa, Out-of-plane behaviour of a full scale stone masonry façade. Part 2: Shaking table tests, Earthq. Eng. Struct. Dyn. 42 (2013) 2097–2111. doi:10.1002/eqe.2314.
[25] D. Liberatore, C. Doglioni, O. AlShawa, S. Atzori, L. Sorrentino, Effects of coseismic ground vertical motion on masonry constructions damage during the 2016 Amatrice-Norcia (Central Italy) earthquakes, Soil Dyn. Earthq. Eng. 120 (2019) 423–435. doi:10.1016/j.soildyn.2019.02.015.
[26] G. De Canio, G. de Felice, S. De Santis, A. Giocoli, M. Mongelli, F. Paolacci, I. Roselli, Passive 3D motion optical data in shaking table tests of a SRG-reinforced masonry wall, Earthquakes Struct. 10 (2016) 53–71. doi:10.12989/eas.2016.10.1.053.
[27] M. Mongelli, I. Roselli, G. De Canio, F. Ambrosino, Quasi real-time FEM calibration by 3D displacement measurements of large shaking table tests using HPC resources, Adv. Eng. Softw. 120 (2018) 14–25. doi:10.1016/j.advengsoft.2016.07.005.
[28] L. Luzi, F. Pacor, R. Puglia, Italian Accelerometric Archive v. 2.3. Istituto Nazionale di Geofisica e Vulcanologia, Dipartimento della Protezione Civile Nazionale., (2017). https://doi.org/10.13127/ITACA.2.3.
[29] F. Mollaioli, O. AlShawa, L. Liberatore, D. Liberatore, L. Sorrentino, Seismic demand of the 2016-2017 Central Italy Earthquakes, Bull. Earthq. Eng. 17 (2019) 5399–5427. doi:10.1007/s10518-018-0449-y.
[30] EC8-1, Eurocode 8: Design of structures for earthquake resistance—Part 1: General rules, seismic actions and rules for buildings, European Committee for Standardization, Brussels, 2004.
[31] G.W. Housner, Spectrum Intensities of Strong Motion Earthquakes, in: Proc. Symp. Earthq. Blast Eff. Struct. EERI, Los Angeles, California, 1952: pp. 21–36.
[32] M. Tomaževič, Earthquake-resistant Design of Masonry Buildings, Imperial College Press, London, 1999.
[33] B. Silva, M. Dalla Benetta, F. Da Porto, C. Modena, Experimental assessment of in-plane behaviour of three-leaf stone masonry walls, Constr. Build. Mater. 53 (2014) 149–161. doi:10.1016/j.conbuildmat.2013.11.084.
[34] A. Borri, G. Castori, M. Corradi, E. Speranzini, Shear behavior of unreinforced and reinforced masonry panels subjected to in situ diagonal compression tests, Constr. Build. Mater. 25 (2011) 4403–4414. doi:10.1016/j.conbuildmat.2011.01.009.
[35] L. Stempniewski, M. Urban, Shaking Table Tests of a Full-Scale Two-Storey Pre-Damaged Natural Stone Building Retrofitted with the Multi-Axial Hybrid Textile System “Eq-Grid,” in: Geotech. Geol. Earthq. Eng., 2014: pp. 155–169. doi:10.1007/978-3-319-00458-7_9.
[36] F. Ferretti, A. Incerti, B. Ferracuti, C. Mazzotti, FRCM Strengthened Masonry Panels: The Role of Mechanical Anchorages and Symmetric Layouts, Key Eng. Mater. 747 (2017) 334–341. doi:10.4028/www.scientific.net/KEM.747.334.
[37] M. Shabdin, M. Zargaran, N.K.A. Attari, Experimental diagonal tension (shear) test of Un-Reinforced Masonry (URM) walls strengthened with textile reinforced mortar (TRM), Constr. Build. Mater. 164 (2018) 704–715. doi:10.1016/j.conbuildmat.2017.12.234.
[38] Ö.S. Türkmen, B.T. De Vries, S.N.M. Wijte, A.T. Vermeltfoort, In-plane behaviour of clay brick masonry wallettes retrofitted with single-sided fabric-reinforced cementitious matrix and deep mounted carbon fibre strips, Bull. Earthq. Eng. 18 (2020) 725–765. doi:10.1007/s10518-019-00596-2.
[39] K.Q. Walsh, D.Y. Dizhur, J. Shafaei, H. Derakhshan, J.M. Ingham, In Situ Out-of-Plane Testing of Unreinforced Masonry Cavity Walls in as-Built and Improved Conditions, Structures. 3 (2015) 187–199. doi:10.1016/j.istruc.2015.04.005.
[40] A. Cascardi, M. Leone, M.A. Aiello, Transversal joining of multi-leaf masonry through different types of connector: Experimental and theoretical investigation, Constr. Build. Mater. 265 (2020) 120733. doi:10.1016/j.conbuildmat.2020.120733.
[41] A. Borri, G. Castori, M. Corradi, R. Sisti, Masonry wall panels with GFRP and steel-cord strengthening subjected to cyclic shear: An experimental study, Constr. Build. Mater. 56 (2014) 63–73. doi:10.1016/j.conbuildmat.2014.01.056.

[42] N. Gattesco, C. Amadio, C. Bedon, Experimental and numerical study on the shear behavior of stone masonry walls strengthened with GFRP reinforced mortar coating and steel-cord reinforced repointing, Eng. Struct. 90 (2015) 143–157. doi:10.1016/j.engstruct.2015.02.024.
[43] N. Gattesco, I. Boem, Out-of-plane behavior of reinforced masonry walls: Experimental and numerical study, Compos. Part B Eng. 128 (2017) 39–52. doi:10.1016/j.compositesb.2017.07.006.
[44] M. Corradi, A. Borri, G. Castori, R. Sisti, The Reticulatus method for shear strengthening of fair-faced masonry, Bull. Earthq. Eng. 14 (2016) 3547–3571. doi:10.1007/s10518-016-0006-5.
[45] F. Longo, A. Cascardi, P. Lassandro, M.A. Aiello, Thermal and Seismic Capacity Improvements for Masonry Building Heritage: A Unified Retrofitting System, Sustainability. 13 (2021) 1111. doi:10.3390/su13031111.
[46] P. Meriggi, G. de Felice, S. De Santis, Design of the out-of-plane strengthening of masonry walls with fabric reinforced cementitious matrix composites, Constr. Build. Mater. 240 (2020) 117946. doi:10.1016/j.conbuildmat.2019.117946.
[47] M. Tondelli, K. Beyer, M. DeJong, Influence of boundary conditions on the out-of-plane response of brick masonry walls in buildings with RC slabs, Earthq. Eng. Struct. Dyn. 45 (2016) 1337–1356. doi:10.1002/eqe.2710.
[48] L. Liberatore, O. AlShawa, C. Marson, M. Pasca, L. Sorrentino, Out-of-plane capacity equations for masonry infill walls accounting for openings and boundary conditions, Eng. Struct. 207 (2020) 110198. doi:10.1016/j.engstruct.2020.110198.
[49] A.W. Phillips, R.J. Allemang, An overview of MIMO-FRF excitation/averaging/processing techniques, J. Sound Vib. 262 (2003) 651–675. doi:10.1016/S0022-460X(03)00116-0.

APPENDIX

Table A.1 Shake table test sequences and main observations for the three walls.

Test #	Record	SF	Label	CC wall	CR wall	UR wall
1	WHN	1.0	WHNa			
2	NRC	0.2	NRC02			Relative motion between top beam and rollers.
3	CNE	0.2	CNE02			
4	AMT	0.2	AMT02			Max relative displacement: 4 mm. Top steel beams and rollers tightened after the test.
5	WHN	1.0	WHNb			
6	NRC	0.4	NRC04			
7	CNE	0.4	CNE04			
8	AMT	0.4	AMT04		Small mortar fragment falls from the top right corner of the external side. The mortar cover of the right-most connector to the foundation is slightly spalled.	
9	WHN	1.0	WHNc			
10	NRC	0.6	NRC06	Minor cracks on the external side at the interface between repointing mortar and stone unit.		Dust and small stone fragments start to fall from the left front corner. Light horizontal cracks detected on the internal side. Vertical crack on the left side
11	CNE	0.6	CNE06			Wide vertical crack on the external side, wide horizontal cracks on the internal side, vertical cracks on lateral side
12	AMT	0.6	AMT06		Hairline cracks on the internal side, possibly present since the beginning	Left corner starts to collapse. Horizontal cracks on the internal side more marked. *Maximum absolute acceleration recorded at the base of the wall (0.45 g).*
13	WHN	1.0	WHNd			
14	NRC	0.8	NRC08	Discharge of mortar dust.		Progressive collapse on the external side. A flexural mechanism is clearly visible.
15	CNE	0.8	CNE08			Monolithic and symmetric out of plane failure of masonry leaves. Vertical connectors keep top beam and overburden hanging from bridge crane. *End of test session.*
16	AMT	0.8	AMT08			
17	WHN	1.0	WHNe			
18	NRC	1.0	NRC10			
19	CNE	1.0	CNE10		Dust discharged from front face	
20	AMT	1.0	AMT10	Horizontal crack over the entire width of the wall. Out of plane rocking response, indicating that the strengthening effectively prevents fragmentation.	Formation of an approximately horizontal crack on both the external and internal sides. Mortar fragments fall down.	
21	WHN	1.0	WHNf			
22	NRC	1.2	NRC12	Development of new cracks near the bottom end of the vertical connectors. Development of two cracks on the plaster of the internal side.	Dust discharged from external side. A stone unit becomes isolated by mortar cracks.	
23	CNE	1.2	CNE12	Widening of existing cracks, mortar fragments fall down, a stone unit gets partially	Approximately vertical crack on the right side, mortar dust and fragments fall down. Cracks on	

				dislodged. Cracks on the internal side widen and plaster fragments fall down. Crack on right lateral side.	the external side widen. Mortar cover over the right-most connector to foundation is spalled further.	
24	AMT	1.2	AMT12	Small fragments fall down and several cracks isolate stone units of external side. New crack on internal side intersects one of existing ones.	Right side crack longer and wider. Two additional quasi-horizontal cracks in upper part of external side. Mortar still bonded to repointing cords.	
25	WHN	1.0	WHNg			
26	NRC	1.4	NRC14	A stone unit and several mortar fragments fall down. Discharged dust compromised 3DVision recording.	Severe damage on right lateral side. In left one a vertical crack develops. Cracks on the external side: branched out in the upper part, horizontal at the base, vertical close to left corner. Cracks on the internal side widen. Mortar still bonded to repointing cords.	
27	CNE	1.4	CNE14	Large plaster fragments and a stone unit fall down. Another stone unit close to the top is dislocated, several stone units isolated by mortar cracks.	Several stone units fall down, especially on the right. No failed cord nor connector.	
28	AMT	1.4	AMT14	Several units of top course on external side fall down. A large unit from the internal side falls down. Wall separated from top beam. *Ultimate limit state conditions achieved. Maximum absolute acceleration recorded at the base of the wall: 1.03 g.*	Several units fall down, the base crack is wider, the wall is deflected at the end of the test. *Ultimate limit state conditions achieved. Maximum absolute acceleration recorded at the base of the wall:(0.99 g.*	
29	WHN	1.0	WHNh			
30	NRC	1.6	NRC16	Additional stone units of top course fall down from both sides. Wall behaving monolithically. Discharged dust partially compromised 3DVision recording	Additional stones from the inner core fall down. Widening of the cracks on the lateral sides. *End of test session.*	
31	CNE	1.6	CNE16	Additional units discharged, top beam and overburden engage crane bridge ropes. Discharged dust partially compromised 3DVision recording. *End of test session*.		